NASA/TM—2003-212488

1100 to 1500 K Slow Plastic Compressive Behavior of NiAl-xCr Single Crystals

J. Daniel Whittenberger
Glenn Research Center, Cleveland, Ohio

Ram Darolia
GE Aircraft Engines, Cincinnati, Ohio

September 2003

The NASA STI Program Office . . . in Profile

Since its founding, NASA has been dedicated to the advancement of aeronautics and space science. The NASA Scientific and Technical Information (STI) Program Office plays a key part in helping NASA maintain this important role.

The NASA STI Program Office is operated by Langley Research Center, the Lead Center for NASA's scientific and technical information. The NASA STI Program Office provides access to the NASA STI Database, the largest collection of aeronautical and space science STI in the world. The Program Office is also NASA's institutional mechanism for disseminating the results of its research and development activities. These results are published by NASA in the NASA STI Report Series, which includes the following report types:

- TECHNICAL PUBLICATION. Reports of completed research or a major significant phase of research that present the results of NASA programs and include extensive data or theoretical analysis. Includes compilations of significant scientific and technical data and information deemed to be of continuing reference value. NASA's counterpart of peer-reviewed formal professional papers but has less stringent limitations on manuscript length and extent of graphic presentations.

- TECHNICAL MEMORANDUM. Scientific and technical findings that are preliminary or of specialized interest, e.g., quick release reports, working papers, and bibliographies that contain minimal annotation. Does not contain extensive analysis.

- CONTRACTOR REPORT. Scientific and technical findings by NASA-sponsored contractors and grantees.

- CONFERENCE PUBLICATION. Collected papers from scientific and technical conferences, symposia, seminars, or other meetings sponsored or cosponsored by NASA.

- SPECIAL PUBLICATION. Scientific, technical, or historical information from NASA programs, projects, and missions, often concerned with subjects having substantial public interest.

- TECHNICAL TRANSLATION. English-language translations of foreign scientific and technical material pertinent to NASA's mission.

Specialized services that complement the STI Program Office's diverse offerings include creating custom thesauri, building customized databases, organizing and publishing research results . . . even providing videos.

For more information about the NASA STI Program Office, see the following:

- Access the NASA STI Program Home Page at ***http://www.sti.nasa.gov***

- E-mail your question via the Internet to help@sti.nasa.gov

- Fax your question to the NASA Access Help Desk at 301–621–0134

- Telephone the NASA Access Help Desk at 301–621–0390

- Write to:
  NASA Access Help Desk
  NASA Center for AeroSpace Information
  7121 Standard Drive
  Hanover, MD 21076

NASA/TM—2003-212488

1100 to 1500 K Slow Plastic Compressive Behavior of NiAl-xCr Single Crystals

J. Daniel Whittenberger
Glenn Research Center, Cleveland, Ohio

Ram Darolia
GE Aircraft Engines, Cincinnati, Ohio

National Aeronautics and
Space Administration

Glenn Research Center

September 2003

The Propulsion and Power Program at
NASA Glenn Research Center sponsored this work.

Available from

NASA Center for Aerospace Information
7121 Standard Drive
Hanover, MD 21076

National Technical Information Service
5285 Port Royal Road
Springfield, VA 22100

Available electronically at http://gltrs.grc.nasa.gov

1100 to 1500 K Slow Plastic Compressive Behavior of NiAl-xCr Single Crystals

J. Daniel Whittenberger
National Aeronautics and Space Administration
Glenn Research Center
Cleveland Ohio 44135

Ram Darolia
GE Aircraft Engines
Cincinnati, Ohio 45215

Abstract

The compressive properties of near <001> and <111> oriented NiAl-2Cr single crystals and near <011> oriented NiAl-6Cr samples have been measured between 1100 and 1500 K. The 2Cr addition produced significant solid solution strengthening in NiAl, and the <111> and <001> single crystals possessed similar strengths. The 6Cr crystals were not stronger than the 2Cr versions. At 1100 and 1200 K plastic flow in all three Cr-modified materials was highly dependent on stress with exponents > 10. The <011> oriented 6Cr alloy exhibited a stress exponent of about 8 at 1400 and 1500 K; whereas both <001> and <111> NiAl-2Cr crystals possessed stress exponents near 3 which is indicative of a viscous dislocation glide creep mechanism. While the Cottrell-Jaswon solute drag model predicted creep rates within a factor of 3 at 1500 K for <001>-oriented NiAl-2Cr; this mechanism greatly over predicted creep rates for other orientations and at 1400 K for <001> crystals.

Introduction

Over the past eight years a considerable amount of work [1-12] has been undertaken on directionally solidified (DS'ed) NiAl+(34-x)Cr+xMo eutectics, where x ranges from 0 to 6 at.%. These studies, which expanded upon the 1970's investigations of Walter and Cline et al. [13-15], were aimed at finding a lower density, higher strength, more oxidation resistant and better thermal conductivity replacement for the current generation of Ni-based superalloys. Such a goal was and still is reasonable, as these eutectics can possess good elevated temperature creep strength (a creep rate of ~10^{-7} s^{-1} at 1300 K and 100 MPa) and an ~20 MPa•√m room temperature toughness [1] which is supplemented by the inherent oxidation resistance [16] and high thermal conductivity [17] of NiAl.

The microstructure and orientation relationships of the two phases in directionally solidified NiAl+(34-x)Cr+xMo eutectics are dependent on the composition [14]. Alloys containing less than ~0.6Mo form micron diameter Cr(Mo) fibers in a NiAl matrix, where both phases have their <001> direction parallel to the growth axis; higher Mo content eutectics, however, solidify as alternating micron thick Cr(Mo) and NiAl lamella which both have <111> axes parallel to the growth direction. While such a change in orientation probably has little importance for the body centered cubic metallic Cr(Mo) phase, it could be significant for B2 crystal structure NiAl, which generally deforms by the motion of <001> Burgers vector dislocations [18]. For example Forbes et al. [19] testing of binary NiAl has shown that hard, <001> crystals creep at a two orders of magnitude slower rate than soft <223> oriented crystals at and below 1473 K.

Based on the known plastic strength properties for NiAl and Cr, one cannot account for the excellent elevated temperature strength of directionally solidified NiAl+34Cr or its Mo-modified versions. At 1300 K and 15 MPa both <001> oriented [1,19] and polycrystalline [20] NiAl and polycrystalline Cr [21] will flow at a rate of ~ 10^{-7} s^{-1} which is about a factor of seven weaker than the directionally solidified eutectics. Although microstructural strengthening has been suggested for the better creep resistance of the directionally solidified eutectics [9–12,22], it is possible that solid solution hardening of Cr(Mo) and/or NiAl has also occurred [4,22], as both phases are slightly soluble in one another [3,8,23,24].

While there is no information on the strength of Cr(Mo) alloys, several studies of alloyed NiAl single crystals do provide evidence that high temperature solid solution strengthening is possible. Walston et al. [25] demonstrated in 1993 that the replacement of Al with small amounts of Cr lead to significant increases in the stress rupture life of 50Ni+(50-x)Al+xCr crystals (x = 2 or 4) at 1255 K-86 MPa compared to binary NiAl single crystals. Additionally, as part of 1273 K creep study of directionally solidified NiAl-(Cr,Mo) eutectics, Kolluru and Pollock [4, 22] tested a few <111> oriented 50Ni-48Al-2Cr single crystals and found that they were much stronger than NiAl crystals.

The best evidence for solid solution hardening of NiAl single crystals to date involves the replacement of a small amount Al with Ti, where Walston et al. [25] indicated that the stress-rupture properties of Ni-47.5Al-2.5Ti samples were significantly greater than that of NiAl. A subsequent creep study of NiAl-2.5Ti single crystals by Kitabjian et al. [26] found that this small Ti addition produced a factor of 6 strength enhancement over Ni-50Al deformed at 1273 K, and more recent work [27] with NiAl-3.6Ti crystals concluded that creep in solid solution <001> oriented NiAl-xTi specimens was consistent with the Cottrell-Jaswon solute-drag model [28,29]. In addition to strengthening, Ti-modifications appeared to have dramatically changed the deformation characteristics of the crystals. While prior work [18,19] on binary NiAl single crystals had shown that "hard" <100> samples are much stronger than "soft" non-<100> crystals, Kitabjian et al. [26] reported that both <100> and <111> NiAl-2.5Ti crystals displayed similar flow stress-strain rate properties between 1173 to 1473 K. This creep behavior in conjunction with the nearly identical stress-rupture results for <100>-, <011>- and <111>-oriented NiAl-2.5Ti crystals [25] reveals a clearly unexpected orientation anisotropy in solid solution alloyed NiAl-based single crystals.

Although Ti- and Cr- solid solution modified NiAl single crystals appear to be strong, their counterpart polycrystalline alloys have been surprisingly weak at elevated temperature. Vedula et al. [30] did not find any significant strength difference between polycrystalline Ni-47.8Al-2.2Ti and NiAl at 1300 K between 10^{-5} and 10^{-7} s^{-1}. Even doubling the Ti content to Ni-45Al-5Ti [31], which is approximately the solid solubility limit, did not improve the 1300 K slower strain rate deformation resistance (< 10^{-6} s^{-1}) of this polycrystalline alloy over that of NiAl. In a similar vein, as-arc melted and heat treated 50Ni+(50-x)Al+xCr alloys with x = 4, 6 and 8 were tested by Han, Tian, and Nemoto [32], and they found that the 0.2% yield strength of these materials were similar to those for NiAl above 1000 K even though the higher Cr content alloys exceeded the solubility limit.

Since any understanding of the behavior of directionally solidified eutectics is dependent on knowledge of the deformation characteristics of each phase, a study of the creep properties of dilute Cr modified NiAl single crystals was initiated. In large part, this effort was possible because of the availability of appropriate crystals which were utilized in [25] and other General Electric Aircraft Engine (GEAE) studies. Compressive creep testing under both constant velocity and constant load conditions was conducted between 1100 and 1500 K on near <100> and <111> oriented NiAl-2Cr samples and near <011> oriented NiAl-6Cr crystals. The resultant mechanical properties were compared to the predictions of existing solid solution strengthening models and the known deformation characteristics of binary NiAl.

Experimental Procedures

Materials

Pieces taken from two different NiAl-Cr single crystals, nominally NiAl-2Cr and NiAl-6Cr, were obtained from GEAE for machining into small compression samples. The original crystals were grown via a modified Bridgman technique [25] to produce approximately 25 by 40 mm in cross section and about 100 mm long slabs which were then annealed in argon for 50 h at 1583 K to reduce local dendritic segregation. Upon receipt, each piece was checked for orientation by the back reflection Laue technique, then placed in a goniometer and appropriately rotated for the machining of <001> oriented compression specimens. Prior to machining the orientation of each goniometer mounted piece was rechecked by a second back reflection Laue pattern.

Depending on the size of the initial pieces of crystal, lengths some 50 to 80 mm long by ~4 mm diameter rods were wire electrodischarged machined (EDM'ed) from each of the compositions and cut into 8 mm long specimens with an as-EDM'ed surface finish on all faces. This latter technique gave slightly out-of-round cross sections due to a wire EDM parting line along the specimen length, where the "out-of-roundness" was at most ± 25 microns out of 4 mm (i.e. ± 0.6 percent).

The orientation of each group of samples was checked by the Laue technique on a randomly selected specimen. While <100> axis was parallel to the sample length for NiAl-2Cr, the NiAl-6Cr specimen was found to have a near <011> orientation. This latter discrepancy was reconfirmed by examination of another NiAl-6Cr specimen; the reason(s) for the mistake in orientation is not known. Although there was insufficient material for another attempt to machine <100> specimens from NiAl-6Cr, sufficient stock existed for the taking of <111> oriented samples from NiAl-2Cr. This was done following the same procedure as that for <100> specimens, and a check of randomly chosen samples indicated that the proper orientation was nearly achieved. Figure 1(a) illustrates the orientation of the as-machined samples taken from each group; in the case NiAl-2Cr, the two tested orientations closely represent the orientation of the NiAl phase in NiAl+(34-x)Cr+xMo eutectics, where $x < 0.6$ results in the [100] orientation and $x > 0.6$ gives the [111] orientation.

Alloy chemistry was determined by destructive analysis of as-machined compression samples, and the measured compositions are given in table 1, where the major elements are reported in atom % and the minor elements in atom parts per million, appm. While all the third element modifications are close to their intended targets, the NiAl-6Cr crystals contain slightly less Si and a higher total amount of minor element impurities compared to NiAl-2Cr.

TABLE 1.—ALLOY CHEMISTRY

Identification	Major constituents, at.%				Minor constituents, appm				
	Al	Cr	Ni	Si	Co	Cu	Fe	Mn	Y
NiAl-2Cr	47.4	1.89	50.5	0.15	----	7	156	8	29
NiAl-6Cr	46.0	5.74	48.0	0.12	445	21	548	24	---

Compression Testing

The 1100–1400 K slow plastic deformation properties in air at strain rates ranging from 10^{-2} s^{-1} to 10^{-7} s^{-1} were determined by compressing samples between solid SiC push bars under constant velocity conditions in a universal testing machine. The autographically recorded load-time charts from the test machine operating at speeds ranging from 2.1×10^{-3} to 2.1×10^{-6} mm/s were converted to true

compressive stresses, strains, and strain rates via the offset method and the assumptions that volume is conserved and all plastic deformation occurred in the specimen.

To compliment the constant velocity testing, strength properties in air at strain rates $\leq 10^{-7}$ s^{-1} between 1100 K to 1400 K and all the compressive properties at 1500 K were measured by constant load compressive creep testing in lever arm creep frames. Creep strain was determined as a function of time through periodic measurements of the relative positions of ceramic push bars applying the force to the specimen. After normalizing the contraction-time results with respect to the final specimen length, the data were converted into true stresses and strains by assuming volume conservation. While most creep specimens were subjected to multiple engineering stress conditions, a few samples were tested under a single load. Steady state creep rates were determined by linear regression techniques applied to the visually selected linear region of the true stress-time data. Such values were then paired to the average true flow stress applied during the steady state regime.

In addition to giving the strength properties at several stresses, multiple constant load testing allowed examination of transient creep after the majority of test frame play had been removed by the initial load application. For this analysis instantaneous strain rates were calculated by stepping five data point linear regression analyses through the entire set of strain-time results and these values were then plotted as functions of time and creep strain.

Results

Constant Velocity Testing

The 1100 through 1400 K stress-strain curves for each alloy- orientation combination are illustrated in figs. 2–5, respectively, as a function of the approximate imposed strain rate. In general these stress-strain curves reveal that (1) strength decreases with a decrease in the imposed strain rate {all parts of figs. 2–5}; (2) strength at any imposed strain rate decreases as the test temperature increases {compare any material-orientation-strain rate combination across figs. 2–5} and (3) a small amount of work hardening takes place over the initial 1 to 2 percent strain before continued flow at a more or less constant stress {best illustrated by Parts (c) of figs. 2–5}. There are exceptions to each of these generalizations: for example, (1) the measured strength levels of <111> NiAl-2Cr are approximately the same at 1100 and 1200 K {figs. 2(b) and 3(b)}; (2) occasional yield points {<001> NiAl-2Cr - 2 x 10^{-3} s^{-1} at 1100 K (fig. 2(a)) and 1200 K (fig. 3(b))}; continuous work hardening {<001> NiAl-2Cr – 2 × 10^{-3} s^{-1} from 1100 to 1400 K (Parts (a) of figs. 2–5} and strain softening {<111> NiAl-2Cr at 1400 K (fig. 5(b))} were observed.

The orientation of three tested crystals was determined after ~16 h constant velocity compression at 1300 K-1.5 × 10^{-6} s^{-1} to ~7 percent strain and is shown in fig. 1(b). Compared to the untested orientations in fig. 1(a) the <001> oriented NiAl-2Cr rotated toward <011>, the near <111> oriented NiAl-2Cr rotated toward <001> and the near <011> NiAl-6Cr rotated away from the <001>.

Constant Load Creep Testing

Creep plots resulting from 1100 to 1500 K testing are given in figs. 6 through 10 respectively, as functions of engineering stress for each alloy-orientation combination. Overall the materials deformed in the usual manner upon initial loading with first stage creep proceeding to a steady state, as is illustrated by the 1400 K-20 MPa creep curve for the <001> oriented NiAl-2Cr sample in fig. 9(a) and its instant-aneous creep rate-time plot in fig. 11(a). Such behavior was seen for all the alloy-orientation-temperature combinations except for <111> oriented NiAl-2Cr specimens creep tested at 1400 K between 20 and

45 MPa (fig. 9(b)); for these tests the initial work hardening was immediately followed by work softening that resulted in very limited steady state regime or a creep rate minimum as illustrated by fig. 11(b).

At any temperature a higher stress lead to more deformation in a shorter time (all parts of figs. 6–10). Occasionally a few specimens did transition from steady state to an apparent third stage creep {for instance <011> oriented NiAl-6Cr at 1200 K-65 MPa (fig.7(c)}. In the cases where multiple constant loading conditions involved a return to the initial engineering stress, the steady state behavior of the initial and repeat loadings appeared to be about the same {for example: <001> oriented NiAl-2Cr tested at 7.5 to 15 to 7.5 MPa at 1500 K (fig. 10(a))}.

Examples of the instantaneous creep rate-creep strain behavior prior to and following a stress change are present in figs. 12–14 as function of creep strain (Parts (a,c)) and time (Parts (b,d)). Basically two distinct patterns were observed for each orientation-NiAl-Cr combination. Application of a higher stress at and below 1300 K resulted in an immediate increase in the strain rate which then slowly decreased due to work hardening as creep continued to occur in terms of strain (figs. 12(a), 13(a)) or time (figs. 12(b), 13(b)). With one exception at 1400 K for <011> oriented NiAl-6Cr samples (fig. 14(a,b)); all load increases (decreases) at either 1400 or 1500 K resulted in the almost instantaneous transition to a higher (lower) constant steady state creep rate with little clear evidence of either work hardening or softening as a function of strain (figs. 12(c), 13(c), and 14(c)) or time (figs. 12(d), 13(d), and 14(d)).

In the cases where work hardening was clearly observed (figs. 12(a,b), 13(a,b), and 14(a,c)), the transition to the new steady state involved the accumulation of strain over a well defined period of time, where for example the 50 to 75 MPa transition in <001> NiAl-2Cr took place over ~50 ks and ~5 percent strain (figs. 12(a,b)) before the new steady state was established, while the 20 to 33 MPa in <011> NiAl-6Cr took place over ~1.4 ks and ~0.4 percent strain (figs. 14(a,b)) before the new steady state was established. This behavior can be contrasted to the sharp transition upon a stress increase shown in (figs. 12(c,d), 13(c,d), and 14(c,d)), where there is almost no strain accumulated (<0.1 percent) or passage of time (<200 s) before the new steady state is established.

A summary of all the creep transitions for the multiple constant load creep tests is given in appendix A.

Strain Rate-Flow Stress-Temperature Behavior

Figure 15 illustrates the dependency of the true compressive strain rate ($\dot{\varepsilon}$) for each alloy-orientation combination on true flow stress (σ) and temperature (T). The open symbol data points represent the flow stresses required to produce 3 percent strain from the stress-strain-temperature diagrams (figs. 2–5) determined under constant velocity test conditions, while the solid symbols indicate steady state creep rate - average stress values from creep testing (figs. 6–10). For documentation purposes the flow stress-strain rate-temperature data for all three forms of NiAl-xCr are given in appendix B.

Where possible, the data were fitted to a temperature compensated power law relationship (eq. (1)) defined by

$$\dot{\varepsilon} = A\,\sigma^{n}\exp(-Q/(RT)), \qquad (1)$$

where A is a constant, n is the stress exponent, Q is the activation energy for deformation and R is the universal gas constant. The values for A, n, Q and the standard deviations for the stress exponent (δ_n) and activation energy (δ_Q) as well as the coefficient of determination (R_d^2) for each fit are given in table 2. The curves in fig. 15 are the result of the linear regression analyses and indicated the range of data utilized for each fit.

Deformation in single crystal NiAl-xCr in figs. 15(a–c) displays two distinct regimes for each alloy-orientation: a lower temperature/higher strain rate grouping with a high stress exponent (~15, table 2) and higher temperature/slower strain rate group with much lower stress exponents (~8 or ~3.5, table 2).

Statistical testing using the dummy variable technique in the linear regression analyses revealed that there was no difference between constant velocity and constant load creep data for the <011> NiAl-6Cr crystals deformed in either regime. No difference in test method also existed for <111> NiAl-2Cr samples compressed in the lower temperature/higher strain rate regime; however, use of the dummy variable, indicated that creep tested <001> NiAl-2Cr crystals were slightly stronger than would be predicted based solely on the constant velocity behavior. Based on the current availability of data, the influence of test method could not be examined for either <001> or <111> NiAl-2Cr specimens in their higher temperature/slower strain rate groups, as only one constant velocity test value was available in these regimes

Comparison of the strength levels of the different Cr compositions and single crystal orientations is shown in fig. 16. Between 1100 and 1400 K the <111> oriented NiAl-2Cr crystals are as strong, and in many instances stronger, that the <001> oriented samples; only at 1500 K does the <001> oriented NiAl-2Cr possess a strength advantage over the <111> oriented alloy. Furthermore both the <001> and <111> oriented NiAl-2Cr crystals are stronger than the <011> oriented NiAl-6Cr between 1100 and 1400 K; however at 1500 K this latter material displays the best strength of all three Cr content-orientation combinations.

TABLE 2.—TEMPERATURE COMPENSATED POWER LAW DESCRIPTIONS OF THE STRAIN RATE-FLOW STRESS-TEMPERATURE BEHAVIOR OF NiAl-xCr SINGLE CRYSTALS

Alloy	Orientation	A, s^{-1}	n	δ_n	Q, kJ/mol	δ_Q,	R_d^2
		(a) Lower temperature-higher strain rate fits					
NiAl-2Cr	<001>[1]	2.24×10^{-17}	17.75	1.09	555.8	42.6	0.918
NiAl-2Cr	<111>	1.83×10^{-14}	13.21	1.46	446.2	53.9	0.845
NiAl-6Cr	<011>	3.02×10^{-14}	13.38	0.35	410.5	42.6	0.991
		(b) Higher temperature-slower strain rate fits					
NiAl-2Cr	<001>	1.22×10^{11}	3.23	0.38	608.0	95.4	0.890
NiAl-2Cr	<111>	4.31×10^{30}	3.67	0.43	1163.5	116.7	0.926
NiAl-6Cr	<011>	1.48×10^{8}	7.71	0.36	687.2	46.7	0.974

[1] The use of a dummy variable indicated that creep tested samples were slightly stronger than the constant velocity specimens. Including the test method as part of the analysis: $\dot{\varepsilon} = \exp(-33.41-2.10X)\,\sigma^{15.0}\exp(-472.8/(RT))$, where X = 1 for creep testing and 0 for constant velocity testing; $\delta_n = 1.19$; $\delta_Q = 42.3$ kJ/mol; and $R_d^2 = 0.946$.

Discussion

As illustrated in fig. 17(a), the data from the current testing of <111> oriented NiAl-2Cr single crystals confirm the preliminary 1273 K results of Kolluru [4]. Both investigations show that a ~2 at.% Cr addition to NiAl greatly improves the strength over that of binary single crystals, and, if anything, more extensive testing indicates that Cr is a better elevated temperature solid solution strengthener than was envisioned by Kolluru et al. [4,22]. Furthermore the results in fig. 17(b) indicate that the properties of

even “hard” oriented NiAl (<001> crystals) can be significantly improved by 2Cr between 1100 and 1500 K, where the strength increases are a factor of 2 or more than those measured by Forbes et al. [19] in binary NiAl.

Orientation

Compared to the results of Forbes et al. [19], who reported that <001> crystals have a strength advantage over other orientations in binary NiAl, small Cr additions to NiAl single crystals appears to have changed the elevated temperature deformation characteristics. This supposition follows from measured strength levels where <111> oriented NiAl-2Cr crystals are as strong, and sometimes even stronger, than <001> NiAl-2Cr samples between 1100 and 1400 K (fig. 16). Similar behavior was also found by Walston et al. [25] and Kitabjian et al. [26] in NiAl-2.5Ti single crystals. In view of these results and Noebe et al. [18] review of the temperature dependency of yield strength of NiAl single crystals, where all crystal orientations possessed essentially equal properties for $T \geq 1000$ K and yield strengths of non-stoichiometric [001]-oriented NiAl crystals converged at ~1000 K, the independence between mechanical strength and orientation for $T \geq 1000$ K could, in fact, be the normal behavior for NiAl single crystals.

Cr Content

As testing the NiAl-2Cr crystals in the hardest orientation (<001>) and one of the weakest orientations (<111>) had little effect on mechanical strength at and above 1100 K, the specific testing direction appears to be immaterial; thus some speculations on the effect of Cr content in NiAl single crystals can be made. Clearly fig. 16 does not reveal any strength advantage between 1100 and 1400 K for tripling the Cr concentration from ~2 to ~ 6 at.%. This independence on Cr content exists even though Tian et al. (24) and Han et al. (32) room temperature hardness testing of 1073 and 1173 K aged samples of several different versions of NiAl-6Cr {Cr substituted for Ni, Cr substituted for Al, and Cr substituted for both Ni and Al in order to maintain Ni/Al = 1} revealed that nanometer sized Cr precipitates were formed during aging which first hardened (~ 1h) and then softening (>24 h) the alloys. Thus, Cr precipitates by themselves do not appear to provide any useful strengthening or detrimental weakening at 1100 and 1200 K in NiAl-6Cr, since the current 1100 and 1200 K flow stress-strain rate data (fig. 15(c)) does not reveal any change in behavior as the strain rate is decreased (i.e. time under test is increased)

There is a change in deformation mechanism of NiAl-6Cr at 1300 K (fig. 15(c)), where n decreases from ~13 to about 8 for strain rates $< 2 \times 10^{-5}$ s^{-1} which would correspond to about 2 h or more at temperature. Per Tian et al. (23), the solid solubility for Cr in NiAl at 1298 K would be about 6 at.%; thus the change in stress exponent could be due to the complete dissolution of all Cr particles which would also be true at 1400 and 1500 K because the solubility of Cr in NiAl increase with temperature (24). For $T \geq 1400$ K the relatively high stress exponent of 8 displayed by <011> NiAl-6Cr crystals is in sharp contrast to the $n \approx 3$ of either <001>- or <111>-NiAl-2Cr (figs. 15(a,b)). In general terms a stress exponent of about 8 in a single phase alloy would be indicative of a dislocation climb creep mechanism in a constant subgrain size material (33), not a solid solution, dislocation glide controlled creep alloy.

The current transient creep behavior for NiAl-6Cr from multiple stress testing gives conflicting results (fig. 14) as to validity of the constant substructure model: all three 1500 K examples (figs. 14(c,d), appendix 1) reveal an instantaneous change in strain rate with a change in stress which is consistent with a constant substructure; however the single 1400 K stress change test demonstrated work hardening (figs. 14(a,b)) which would signify an evolving substructure. While examples of substructure formation [19, 20, 34] and a constant subgrain size affecting strength [35] during elevated temperature, slow deformation

rate creep exist for binary NiAl, transmission electron microscopy crystals would be required to examine this conjecture in crept <011> NiAl-6Cr single crystals.

At and below 1300 K all three single crystals (fig. 15, table 2) exhibit high stress exponents presumeably due to dislocation interactions and, in the case of NiAl-6Cr, Cr particles which also interfere with the movement of dislocations. Although the n > 10 regimes have no specific deformation mechanism, the n ~ 3 behavior of both NiAl-2Cr crystals at 1400 and 1500 K (fig. 15(a,b), table 2) is believed to be indicative of viscous glide creep, as was the case for 1300–1500 K creep in solid solution NiAl-xTi single crystals [27]. Figure 18 contrasts the behavior of the current <001> oriented NiAl- 2Cr samples to that of <001> NiAl-3.6Ti single crystals. While alloying with 3.6Ti is superior to 2Cr at 1100 and 1200 K, at 1300 K and strain rates below 10^{-6} s^{-1} (fig. 18(a)), the roles reverse when the Ti-modified alloy undergoes n ≈ 3 deformation. At 1400 and 1500 K both alloys display a stress exponent ≈ 3 for strain rates < 10^{-4} s^{-1} (fig. 18(b), table 2, [27]), where strength levels of the two <001> single crystals are about the same in spite of the factor of almost two difference in alloying content.

In addition to a stress exponent of about 3 (figs. 15(a,b), table 2), the two current NiAl-2Cr crystal orientations do not show any sign of work hardening (figs. 12(c,d), 13(c,d), appendix 1) following stress change during a creep test which is the same behavior as that displayed by <001> NiAl-3.6Ti samples [27]. Thus it is reasonable to apply the same Cottrell-Jaswon solute-drag, viscous creep model to NiAl-2Cr crystals that was successfully applied to [001]-oriented NiAl-xTi [27]. The Cottrell-Jaswon steady state creep rate [25], $\dot{\varepsilon}_{CJ}$, is given by

$$(\dot{\varepsilon}_{CJ} kT/(D\mu b)) = (1/(3e^2c)) \cdot (kT/(\mu b^3))^2 \cdot (\sigma/\mu)^3 , \qquad (2)$$

where k is Boltzmann's constant, D is the volume diffusion coefficient, μ is the temperature dependent shear modulus, b is the magnitude of the Burgers vector, e is the linear solute-solvent size difference, and c is the Cr concentration in mole fraction. From table 1 and following [27]

$$c = 0.0189$$
$$D(m^2/s) = 2.98 \times 10^{-5} \exp(-288.5/(RT)), [36];$$
$$\mu(GPa) = C_{44}(T) = 113.15 - 0.02631 \cdot (T-273), [37]; \text{ and}$$
$$b = 0.4077 \text{ nm } \{\mathbf{b} = a_0[110]\} \text{ for [001]-oriented crystals, or}$$
$$b = 0.2883 \text{ nm } \{\mathbf{b} = a_0[100]\} \text{ for non-[001]-oriented crystals.}$$

An exact value for the linear solute-solvent size difference is not known, but it can be estimated through Kitabjian and Nix's lattice parameter procedure [38] using predictions of the effect of Cr on the lattice parameter of NiAl [39]. This method gives an e of –0.041 for Cr in NiAl which is felt to be reasonable as Kitabjian and Nix [38] demonstrated that Bozzolo et al. lattice parameter predictions [39] for Ti in NiAl were accurate to within 20 percent.

The predictions of the Cottrell-Jaswon steady state creep are illustrated along with the flow stress-strain rate data for <001> and <111> NiAl-2Cr single crystals at 1400 and 1500 K in fig. 19. For the [001]-oriented crystals (fig. 19(a)) with $\mathbf{b} = a_0[110]$, the predicted Cottrell-Jaswon creep rates are within a factor of 3 of the measured properties at 1500 K, but the 1400 K predictions are significantly faster (> 50 times) than the actual results. Furthermore the calculated Cottrell-Jaswon creep rates are considerably greater than measured for the [111]-oriented material at either 1400 or 1500 K (fig. 19(b)), where $\mathbf{b} = a_0[100]$. Thus in its present formulation, the Cottrell-Jaswon model does not reflect the observed temperature dependency in NiAl-2Cr crystals as given by the very high activation energies for deformation (> 600 kJ/mol, table 2(b)). Because the inability of this mechanism to estimate creep rates is not uniform, it is unlikely that the choice of the constants (i.e.: c, b, or e) in eq. (2) is solely at fault. Additionally, since comparison of the diffusion coefficients [27] from Ni tracer, interdiffusion in binary, and third element interdiffusion in NiAl has shown that the slowest rates at 1400 and 1500 K would at

most involve a 40 percent reduction from those predicted by Frank et al. [36], a different choice for D can not greatly reduce $\dot{\varepsilon}_{CJ}$. The remaining term in eq. (2), shear modulus, also should not be the source of this discrepancy, as the Young's modulus measurements of Walston and Darolia [17] for NiAl single crystal alloys indicated that neither the modulus value nor temperature dependence was affected by small changes in composition. Thus there is nothing in the formulation of the Cottrell-Jaswon model or in the specific characteristics governing Cr in NiAl which can account for or be the source of the very high activation energies for deformation calculated from the 1400–1500 K deformation of NiAl-2Cr single crystals.

There are four other viscous glide creep mechanisms in the literature [40,41]; of these the destruction of short range order (Fisher interaction) would not be applicable in a B2 crystal structure alloy. It is, however, possible to have stress induced ordering of the solute atoms (Snoek effect), solute enhancement on extended dislocations (Suzuki effect) that inhibits gliding on a plane and an increase in antiphase boundary area due to the motion of non-planer partial dislocations in an ordered alloy. Mohamed [41] has discussed these possible viscous glide mechanisms, and they all depend on the same diffusion parameter as the Cotrell-Jaswon model; hence none of the gliding mechanisms should lead to currently observed high activation energies for deformation (table 2(b)) which are from 2 to 4 times that for Ni tracer diffusion in NiAl [36]. Thus, while the dominate creep process in <001>- and <111>-oriented NiAl-2Cr single crystals appears to be viscous dislocation glide controlled; the exact mechanism is uncertain.

Directionally Solidified NiAl-Cr Eutectics

The current study has shown that a small Cr addition in single crystals does provide a significant solid solution strengthening in comparison to binary NiAl (fig. 17) and that elevated temperature strength is not strongly dependent on orientation. With the assumption that replacement of a small amount of Cr by Mo has little influence on behavior, these two findings suggest that (1) there would be no strength penalty when the NiAl matrix switches from an <001> orientation to a <111> orientation in directionally solidified NiAl-(34-x)Cr-xMo for x >0.6 at.% and (2) the inherent properties of the NiAl matrix within DS'ed NiAl-Cr/Mo eutectics provides a large measure of the overall strength of the eutectics. The first of these two claims has already been confirmed [12], where both directionally solidified NiAl-34Cr and NiAl-33Cr-1Mo eutectics were shown to possess equivalent 1300 K creep properties. The effect of the second claim can be envisioned from fig. 20 which compares the compressive flow strength-strain rate characteristics of DS'ed NiAl-33Cr-1Mo (25.4 mm/h) to those for <111>-oriented NiAl-2Cr between 1200 and 1400 K. While the DS'ed alloy is stronger at faster strain rates, it appears that at all three temperatures and slow strain rates ($<10^{-7}$ s^{-1}) that the strength of the DS'ed eutectic reduces to that of the single phase, solid solution hardened NiAl-2Cr. Therefore, in the 1200–1400 K slower strain rate regimes for DS'ed NiAl-(34-x)Cr-xMo the likelihood of significant solid solution strengthening of (Cr,Mo) or significant microstructural strengthening of either (Cr,Mo) or NiAl alloyed with Cr and Mo seems small. In the case of the Cr(Mo) phase, at best, its strength would be equivalent to that of the NiAl-2Cr, since the overall creep strength of DS'ed NiAl-(34-x)Cr-xMo is equal to that of the solid solution strengthened NiAl-2Cr single crystal phase, which comprises about 65 vol% of the DS'ed eutectic.

Summary of Results

The 1100–1500 K slow strain rate plastic compressive properties of near <001> and <111> oriented NiAl-2Cr single crystals, as well as near <011> oriented NiAl-6Cr samples, have been measured to gain some understanding of the behavior of the matrix phase of directionally solidified NiAl-(34-x)Cr-xMo [$x \leq 6$] eutectics. Testing indicated that an ~ 2 at.% Cr addition provides significant solid solution strengthening to NiAl single crystals, where strength improvements of 2 or more were found, and the <111> oriented alloy was as strong as, and in some cases stronger than, <001> crystals. In addition to strength being apparently independent of orientation, increasing the Cr level to ~6 percent did not provide any additional hardening over the 2 Cr addition. However at 1400 and 1500 K the <011> oriented 6Cr alloy exhibited a stress exponent of about 8; whereas both <001> and <111> NiAl-2Cr crystals possessed stress exponents near 3. At 1100 and 1200 K plastic flow in all three Cr-modified materials was highly dependent on stress with exponents > 10. The nearly immediate transitions to steady state creep after stress change experiments and stress exponents of about 3 strongly suggest that creep in NiAl-2Cr crystals at 1400 and 1500 K occurs by viscous dislocation glide. While the predicted Cottrell-Jaswon solute drag mechanism creep rates were within a factor of 3 of the observed 1500 K creep rates for <001> crystals, the Cottrell-Jaswon mechanism grossly over predicted at 1400 K and for other orientations. Such over predictions were a reflection of very high activation energies for deformation (> 600 kJ/mol) in both NiAl-2Cr single crystal orientations.

References

1. D.R. Johnson, X.F. Chen, B.F. Oliver, R.D. Noebe, and J.D. Whittenberger, *Intermetallics* **3** (1995) 99–113.
2. T.M. Pollock and D. Kollura, Micromechanics of Advanced Materials, eds. S.N.G. Chu, P.K. Law, R.J. Arsenault, K. Sadananda, K.S. Chan, W.W. Gerberich, C.C. Chau, and T.M. Kung, TMS, Warrendale, PA, 1995, pp. 205–212.
3. J. M. Yang, S. M. Jeng, K. Bain, and R. A. Amato, *Acta Mater.*, **45** (1997) 295–305.
4. D.V. Kollura, "The creep deformation of directionally solidified NiAl-Cr and NiAl-Cr(Mo) eutectics," PhD thesis, Dept. of Material Science and Engineering, Carnegie Mellon University, Pittsburgh, PA, 1997.
5. S. V. Raj, I. E. Locci and J. D. Whittenberger, Creep Behavior of Advanced Materials for the 21st Century (edited by R. S. Mishra, A. K. Mukherjee, and K. Linga Murty), TMS, Warrendale, PA, 1999, pp. 295–310.
6. J.D. Whittenberger, S.V. Raj, I.E. Locci, and J.A. Salem. *Intermetallics*, **7** (1999) 1159–1168.
7. S.V. Raj and I.E. Locci, *Intermetallics*, **9** (2001) 217–27.
8. W.S. Walston and R. Darolia, Structural Intermetallics 2001, eds. K.J. Hemker, D.M. Dimiduk, H. Clemens, R. Darolia, H. Inui, J.M. Larsen, V.K. Sikka, M. Thomas, J.D. Whittenberger, TMS, Warrendale, PA, 2001, pp. 735–744.
9. J.D. Whittenberger, S.V. Raj, I.E. Locci, and J.A. Salem. Structural Intermetallics 2001 (eds. K.J. Hemker, D.M. Dimiduk, H. Clemens, R. Darolia, H. Inui, J.M Larsen, S.K. Sikka, M. Thomas, and J.D. Whittenberger) TMS, Warrendale, PA, 2001, pp.775–784.
10. S.V. Raj, I.E. Locci and J.D. Whittenberger, Structural Intermetallics 2001, eds. K.J. Hemker, D.M. Dimiduk, H. Clemens, R. Darolia, H. Inui, J.M. Larsen, V.K. Sikka, M. Thomas, J.D. Whittenberger, TMS, Warrendale, PA, 2001, pp. 785–794.
11. J. Daniel Whittenberger, S.V. Raj, I.E. Locci. Creep Deformation: Fundamentals and Applications (eds. R. S. Mishra, J.C. Earthman, and S.V. Raj) TMS, Warrendale, PA, 2002, pp. 331–341.
12. J. Daniel Whittenberger, S.V. Raj, I.E. Locci, and J.A. Salem, *Metal. Mater. Trans. A.* **33A** (2002) 1385–1397.
13. J. L. Walter and H. E. Cline, *Metall. Trans.* **1** (1970) 1221–1229.
14. H. E. Cline and J. L. Walter, *Metall. Trans.* **1** (1970) 2907–2917.
15. H. E. Cline, J. L. Walter, E. Lifshin, and R. R. Russell, *Metall. Trans.*, **2** (1971) 189–194.
16. J.A. Nesbitt and C.A.. Barrett, *Structural Intermetallics*, R. Darolia, J.J. Lewandowski, C.T. Liu, P.L.Martin, D.B. Miracle, and M.V. Nathal, TMS, Warrendale, PA, 1993, pp. 601-609.
17. W.S. Walston and R. Darolia, High-Temperature Ordered Inter metallic Alloys V, Vol. **288**, (eds I. Baker, R. Darolia, J.D.Whittenberger, and M.H. Yoo), Materials Research Society, Pittsburgh, PA, 1993, pp. 237–242.
18. R.D. Noebe, R.R. Bowman, and M.V. Nathal, *Inter. Mater. Rev*. **38** (1993) 193–232.
19. K.R. Forbes, U. Glatzel, R. Darolia, and W.D. Nix, *Metal. Mat. Trans.* A **27A** (1996) 1229–40.
20. J.D. Whittenberger, *J. Mat. Sci.* **22** (1987) 394–402.
21. J.R. Stephens and W.D. Klopp, *J. Less Com. Metals* **27** (1972) 87–94.
22. D.V. Kollura and T.A. Pollock, *Acta mater*. **46** (1998) 2859–2876.
23. J.D. Cotton, R.D. Noebe and M.J. Kaufman, Structural Intermetallics, (eds. R. Darolia, J.J. Lewandowski, C.T. Liu, P.L. Martin, D.B. Miracle, and M.V. Nathal) TMS, Warrendale, PA 1993, pp. 513–22.
24. W.H. Tian, C.S. Han, and M. Nemoto, *Intermetallics* **7** (1999) 59–67.
25. W.S.Walston, R.D. Field, J.R. Dobbs, D.F. Lahrman, and R. Darolia: Structural Intermetallics, (eds. R. Darolia, J.J. Lewandowski, C.T. Liu, P.L. Martin, D.B. Miracle, and M.V. Nathal) TMS, Warrendale, PA, 1993, pp. 523–532.

26. P.H. Kitabjian, A. Garg, R.D. Noebe, and W.D. Nix, *Metal. Mater. Trans. A* **30A** (1999) 587–600.
27. J. Daniel Whittenberger, Ronald D. Noebe, and Ram Darolia, Elevated temperature creep deformation in solid solution <001> NiAl-xTi single crystals. Submitted to *Mater. Sci. Eng. A*
28. A.H. Cottrell and M.A. Jaswon, *Proc. R. Soc*. **A199** (1949) 104–14 **.**
29. F.A. Mohamed and T.G. Langdon, *Acta Metall*. **22** (1974) 779–88.
30. K. Vedula, V. Pathare, I. Aslandis, and R.H. Titran, High-Temperature Ordered Intermetallic Alloys, vol. **39**, Materials Research Society, Pittsburgh, PA, 1985, pp.411–21.
31. J.D.Whittenberger, R.K. Viswanadham, S.K. Mannan, and K.S. Kumar. *J. Mat. Res*. **4** (1989) 1164–71.
32. C.S. Han, W.H. Tian, and M. Nemoto: Aspects of High Temperature Deformation and Fracture in Crystalline Materials (eds. Y. Hosoi, H. Yoshinaga, H. Oikawa, and K. Maruyama) The Japan Institute of Metals, Aramaki Aoba, Aoba-ku, Sendai 980, Japan, 1993, pp. 195–202.
33. O.D. Sherby, R.H. Klundt, and A.K. Miller, *Met. Trans. A* **8A** (1977) 843–50.
34. J.D. Whittenberger, R. K. Viswanandham, S.K. Mannan, and B. Sprissler, *J. Mat. Sci.* **35** (1990) 35–44.
35. J.D. Whittenberger, *J. Mat. Sci.* **23** (1988) 235–40.
36. St. Frank, S.V. Divinski, U. Södervall, and Chr. Herzig, *Acta mater*. **49** (2001) 1399–1411.
37. Rusovic' and H. Warlimont, *phys. stat sol.* (*a)* **44** (1977) 609–619.
38. P.H. Kitabjian and W.D. Nix, *Acta mater*. **46** (1988) 701–710.
39. G. Bozzolo, R.D. Noebe, and F. Honecy, *Intermetallics* **8** (2000) 7–18.
40. J. Weertman, *Trans. AIME* **218** (1960) 207–218.
41. F.A. Mohamed, *Mater. Sci. Eng. A* **61** (1983) 149–65.

Appendix A.
Type of Creep Transient Observed Following an Engineering Stress Change During Constant Load Creep Testing of NiAl-xCr Single Crystals

Temperature K	Previous stress, MPa	New stress, MPa	Type of transient
	(a) NiAl-Cr <001> orientation		
1100	80	116	Work hardening
1200	65	93	Work hardening
1200	93	128	Work hardening
1200	80	108	Work hardening
1300	50	75	Work hardening
1400	10	16	Instantaneous
1400	16	30	Instantaneous
1500	7.5	15	Instantaneous
1500	15	7.5	Instantaneous
1500	5	10.4	Instantaneous
	(b) NiAl-2Cr <111> orientation		
1100	75	111	Work hardening
1100	111	147	Work hardening
1200	80	98	Work hardening
1200	98	134	Work hardening
1300	30	44	Work hardening
1300	44	66	Work hardening
1400	25	35	Work softening
1500	7.5	12.5	Instantaneous
	(c) NiAl-6Cr <011> orientation		
1100	65	92	Work hardening
1200	50	65	Work hardening
1400	20	33	Work hardening
1500	10	17	Instantaneous
1500	10	26	Instantaneous
1500	13	34	Instantaneous

Appendix B.
Temperature-Strain Rate-Flow Stress Data From Compression Testing of NiAl-xCr Single Crystals

Temperature, K	Strain rate, s^{-1}	Constant velocity testing flow stress, MPa	Constant load creep testing average steady state stress, MPa
		(a) <001> oriented NiAl-2Cr	
1100	2.39E-03	219.0	
1100	2.50E-04	174.7	
1100	2.32E-05	130.9	
1100	1.65E-06	114.3	
1100	4.78E-08		110.2
1100	2.29E-07	106.1	
1100	8.43E-10		79.3
1200	2.17E-03	149.4	
1200	2.29E-04	116.6	
1200	2.21E-05	105.0	
1200	3.98E-06		101.8
1200	1.66E-06	93.7	
1200	2.80E-08		90.4
1200	2.34E-07	79.0	
1200	2.59E-09		79.3
1200	1.23E-09		65.0
1300	2.08E-03	113.4	
1300	2.34E-04	92.4	
1300	1.95E-05	83.2	
1300	1.36E-06	74.6	
1300	1.74E-07	68.4	
1300	1.04E-07		69.6
1300	1.04E-07		60.1
1300	5.38E-09		49.5
1300	1.33E-09		49.9
1400	2.11E-03	85.3	
1400	2.02E-04	76.1	
1400	2.07E-05	68.4	
1400	1.52E-06	61.2	
1400	1.83E-07		39.1
1400	2.41E-07		29.1
1400	4.65E-08		19.7
1400	1.93E-08		15.5
1400	3.06E-09		9.9
1500	1.06E-06		19
1500	3.80E-07		14
1500	3.88E-07		10
1500	2.74E-08		7.2
1500	1.25E-08		6.9
1500	3.20E-08		4.9

Appendix B.—Continued.
Temperature-Strain Rate-Flow Stress Data From Compression Testing of NiAl-xCr Single Crystals

Temperature, K	Strain rate, s^{-1}	Constant velocity testing flow stress, MPa	Constant load creep testing average steady state stress, MPa
	(b) <111> oriented NiAl-2Cr		
1100	2.32E-03	182.3	
1100	2.35E-04	166.1	
1100	2.19E-05	150.8	
1100	1.69E-06	141.4	
1100	2.61E-07	130.3	
1100	1.31E-07		142.4
1100	1.74E-09		110.4
1100	4.01E-10		74.9
1200	2.00E-03	150.7	
1200	2.37E-04	140.2	
1200	2.31E-05	132.3	
1200	2.06E-05	120.3	
1200	4.10E-06		126.4
1200	1.86E-06	129.0	
1200	2.23E-07	113.3	
1200	4.05E-09		97.5
1200	1.10E-10		79.9
1300	2.04E-03	142.1	
1300	2.27E-04	118.8	
1300	2.10E-05	111.4	
1300	1.91E-06	103.7	
1300	2.22E-07	81.3	
1300	4.48E-08		63.6
1300	2.07E-09		43.8
1400	2.48E-03	120.5	
1400	2.16E-04	105.2	
1400	1.83E-05	100.5	
1400	1.22E-06	72.3	
1400	1.23E-07		44.8
1400	2.18E-07		34.3
1400	3.24E-08		29.9
1400	2.16E-08		24.8
1400	6.92E-09		19.9
1500	9.28E-06		18.6
1500	6.90E-07		12.4
1500	6.56E-07		9.6
1500	1.07E-07		7.3
1500	8.00E-08		4.8

Appendix B.—Concluded.
Temperature-Strain Rate-Flow Stress Data From Compression Testing of NiAl-xCr Single Crystals

Temperature, K	Strain rate, s^{-1}	Constant velocity testing flow stress, MPa	Constant load creep testing average steady state stress, MPa
		(c) <011> oriented NiAl-6Cr	
1100	2.46E-03	185.2	
1100	2.54E-04	149.8	
1100	2.28E-05	129.6	
1100	1.68E-06	110.8	
1100	2.14E-07	94.9	
1100	9.94E-08		88.3
1100	2.14E-09		64.2
1200	2.23E-03	147.6	
1200	2.25E-04	119.1	
1200	2.28E-05	100.7	
1200	1.60E-06	85.2	
1200	2.18E-07	75.3	
1200	6.60E-08		63.2
1200	2.13E-09		49.9
1300	2.03E-03	109.4	
1300	2.20E-04	91.4	
1300	2.14E-05	74.4	
1300	1.43E-06	58.3	
1300	2.19E-07	45.9	
1300	1.20E-08		29.7
1400	1.89E-03	78.1	
1400	2.00E-04	60.4	
1400	2.23E-05	47.6	
1400	1.55E-06	37.5	
1400	1.28E-06		32.0
1400	1.43E-08		19.9
1500	6.40E-05		32.9
1500	1.30E-05		24.1
1500	8.77E-07		16.2
1500	3.53E-08		12.9
1500	1.58E-08		9.8

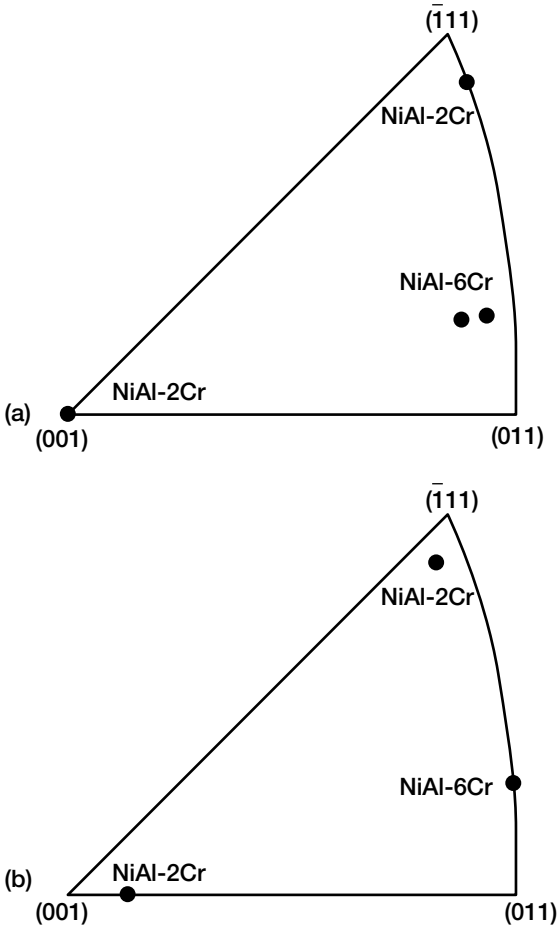

Figure 1.—Sterographic triangles illustrating the orientation of each set of compression samples, (a) as machined, (b) after being tested at 1300 K and a strain rate of ~1.5×10^{-6} s^{-1} to about 7% strain.

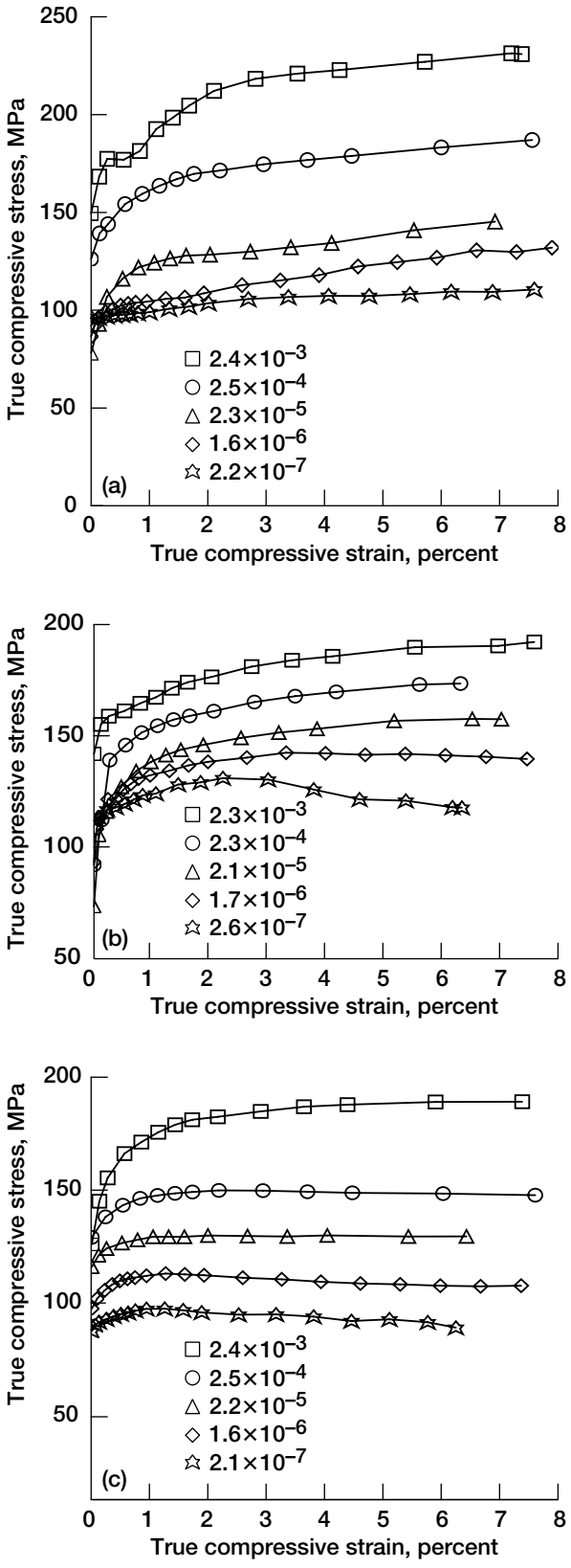

Figure 2.—The 1100 K stress–strain curves as a function of the nominally imposed strain rate. (a) <001> NiAl-2Cr. (b) <111> NiAl-2Cr. (c) <110> NiAl-6Cr.

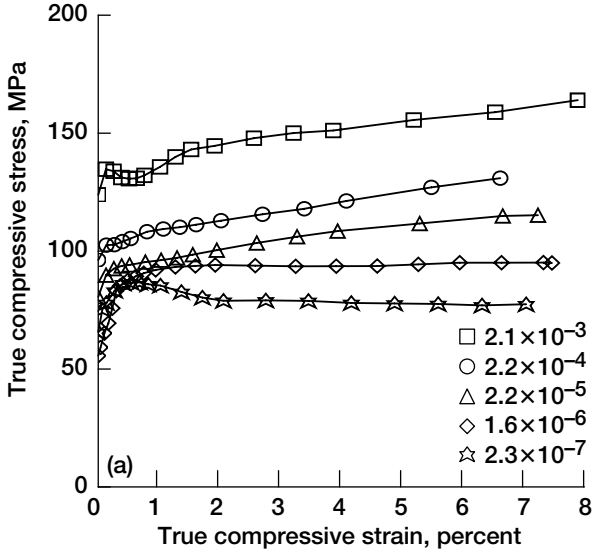

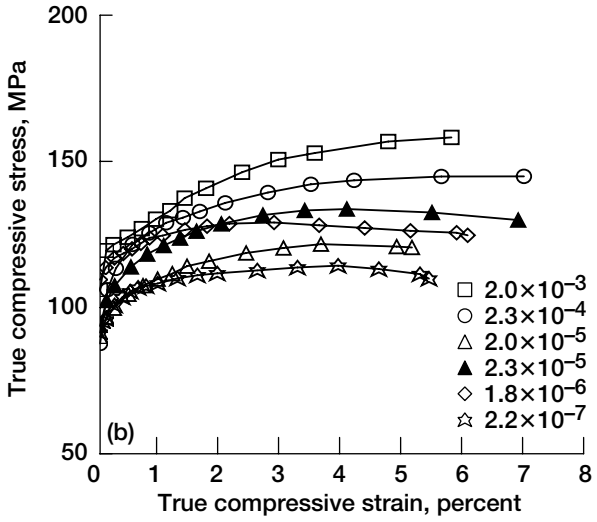

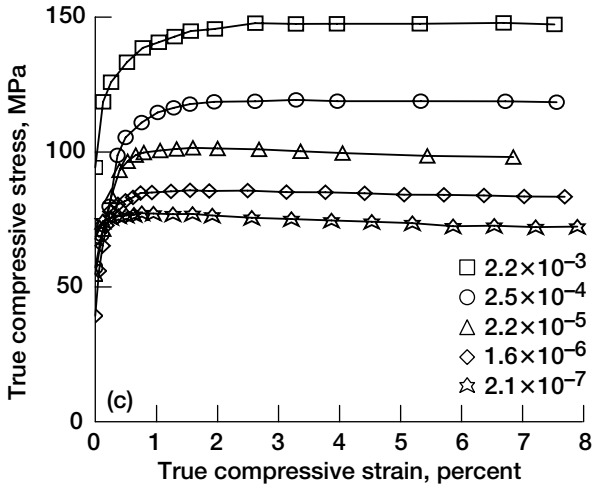

Figure 3.—The 1200 K stress–strain curves as a function of the nominally imposed strain rate. (a) <001> NiAl-2Cr. (b) <111> NiAl-2Cr. (c) <110> NiAl-6Cr.

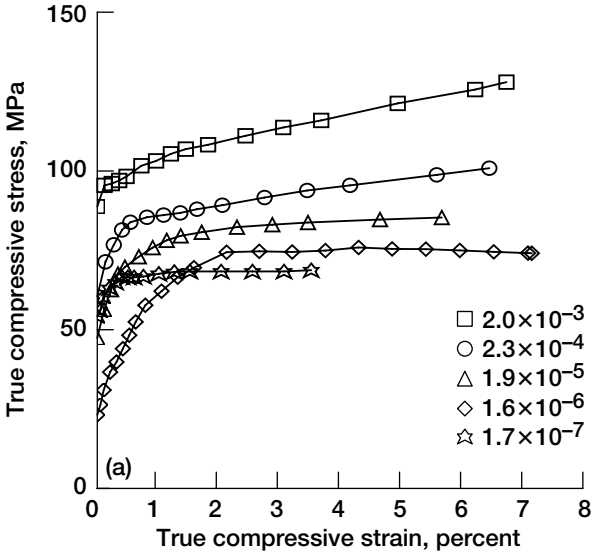

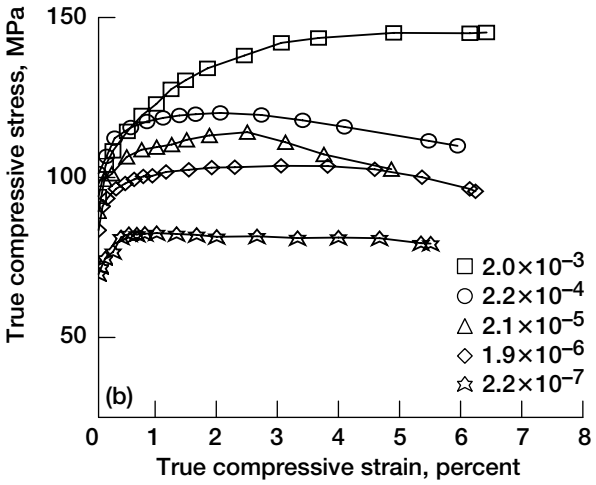

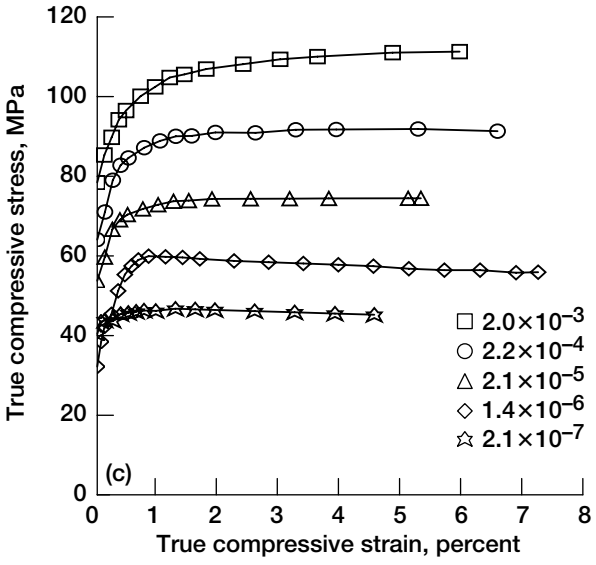

Figure 4.—The 1300 K stress–strain curves as a function of the nominally imposed strain rate. (a) <001> NiAl-2Cr. (b) <111> NiAl-2Cr. (c) <110> NiAl-6Cr.

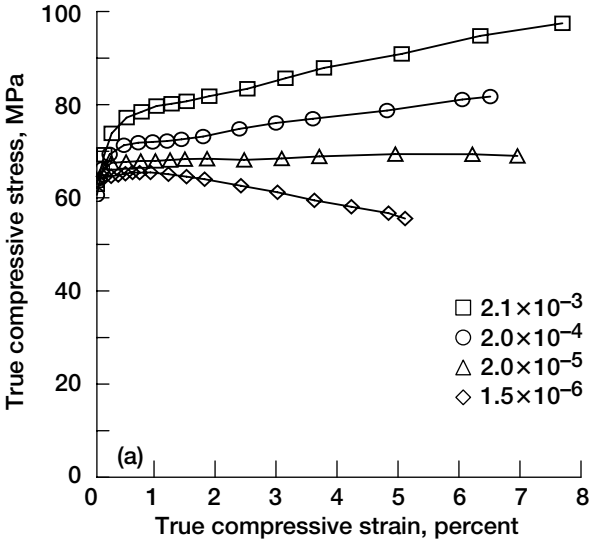

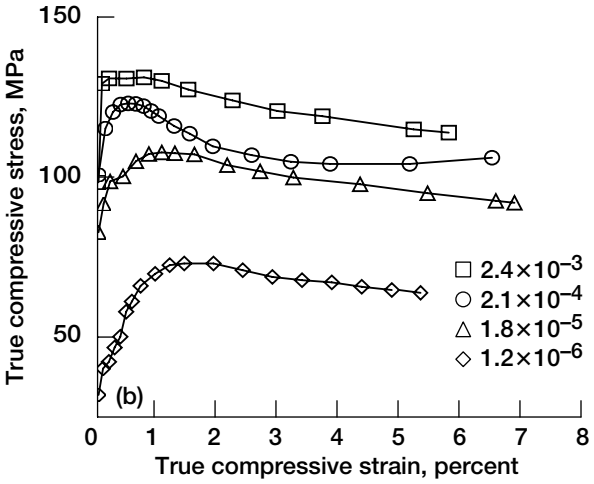

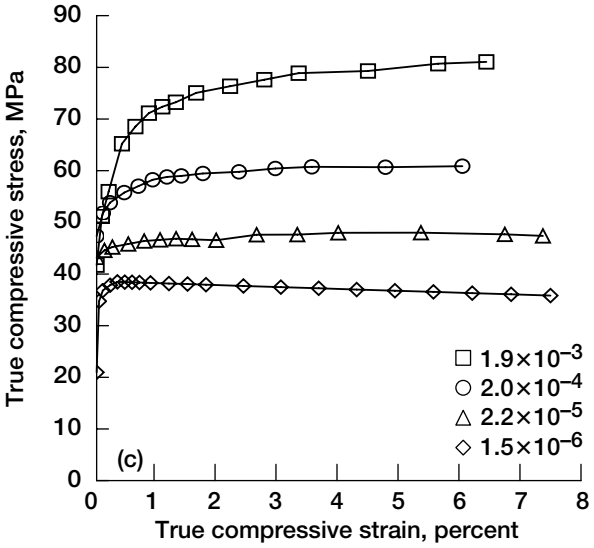

Figure 5.—The 1400 K stress–strain curves as a function of the nominally imposed strain rate. (a) <001> NiAl-2Cr. (b) <111> NiAl-2Cr. (c) <110> NiAl-6Cr.

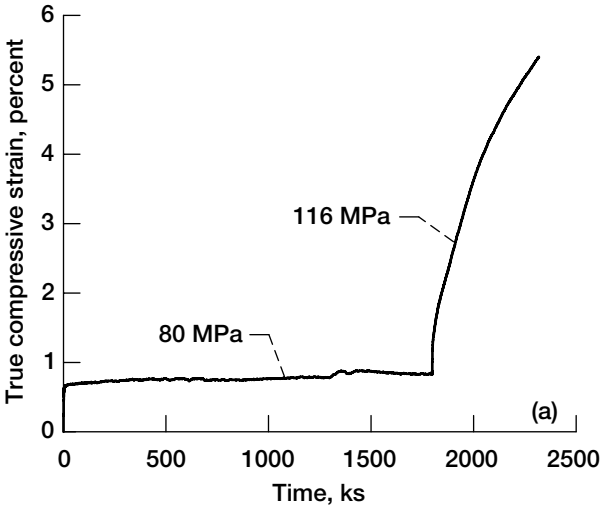

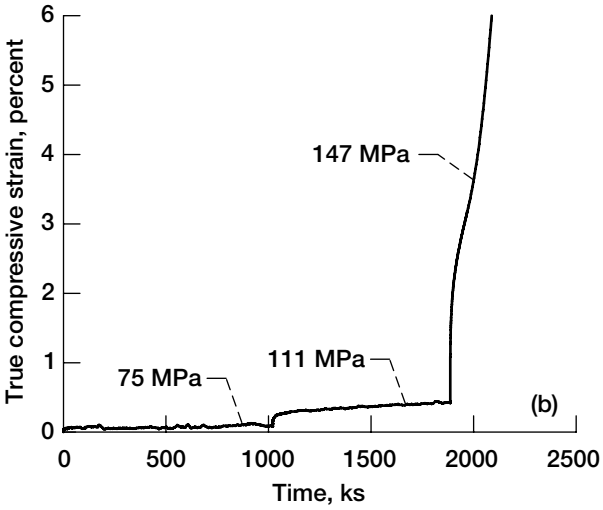

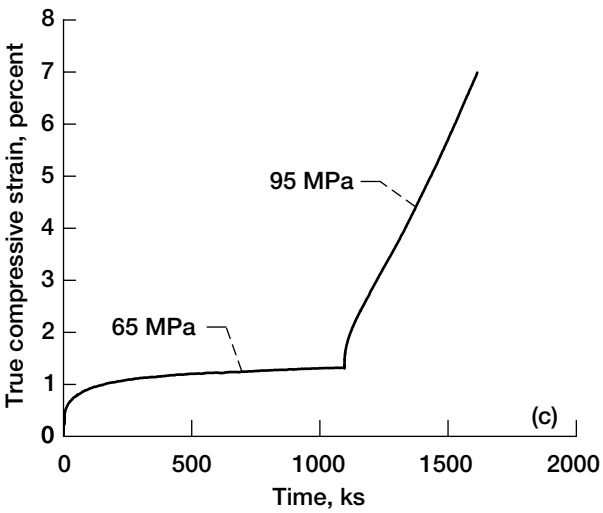

Figure 6.—Multiple constant load creep curves at 1100 K as a function of the engineering stress. (a) <001> NiAl-2Cr. (b) <111> NiAl-2Cr. (c) <110> NiAl-6Cr.

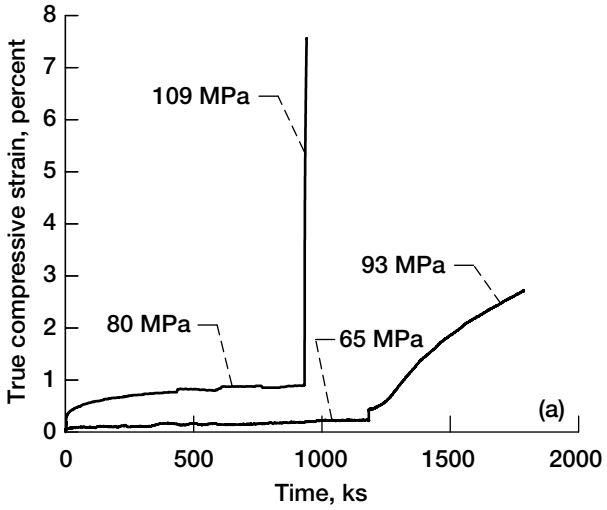

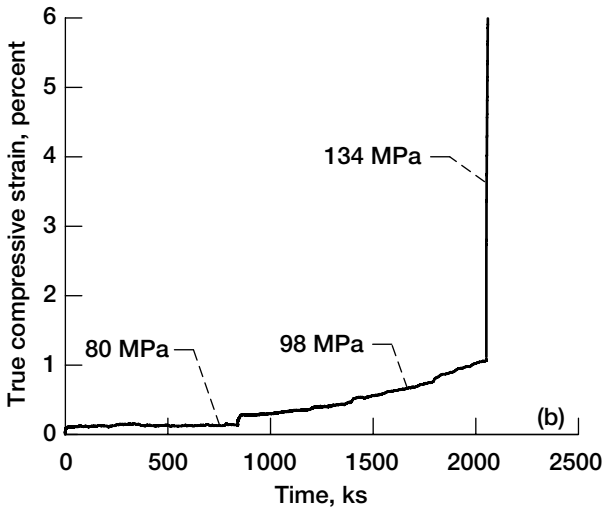

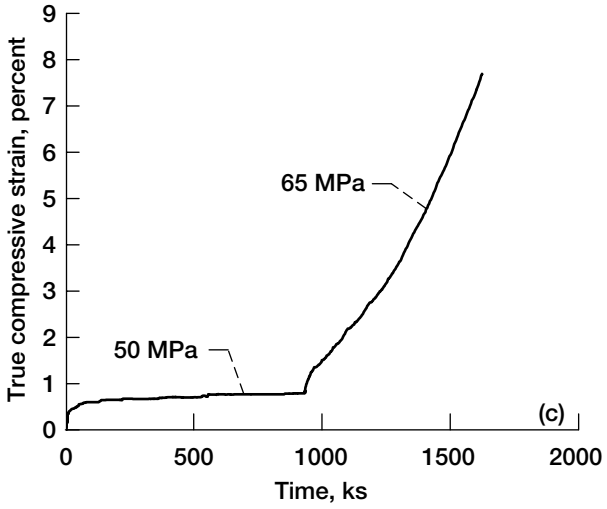

Figure 7.—Multiple constant load creep curves at 1200 K as a function of the engineering stress. (a) <001> NiAl-2Cr. (b) <111> NiAl-2Cr. (c) <110> NiAl-6Cr.

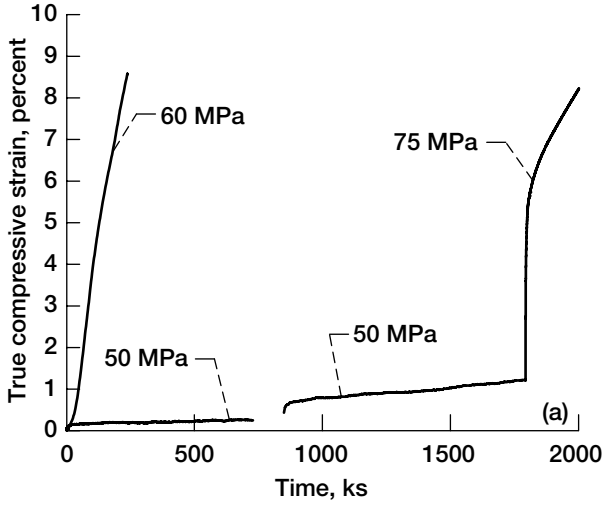

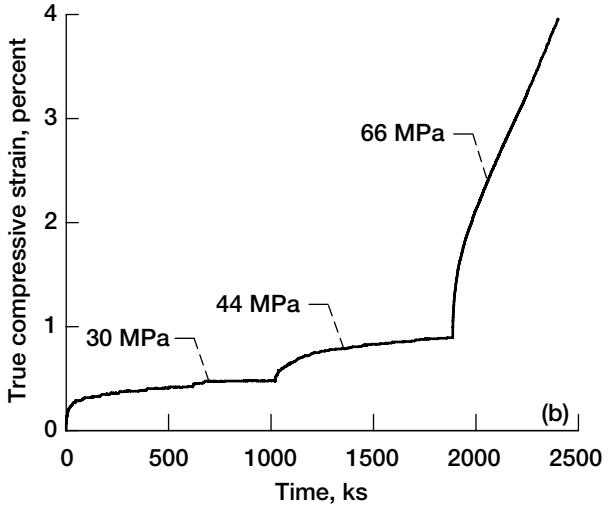

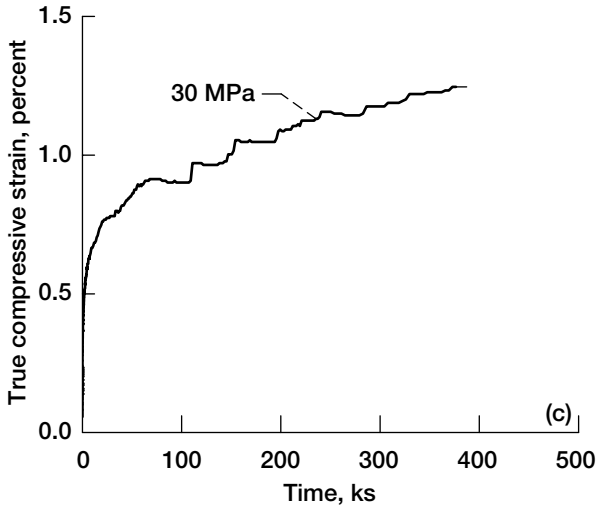

Figure 8.—Single and multiple constant load creep curves at 1300 K as a function of the engineering stress. (a) <001> NiAl-2Cr. (b) <111> NiAl-2Cr. (c) <110> NiAl-6Cr.

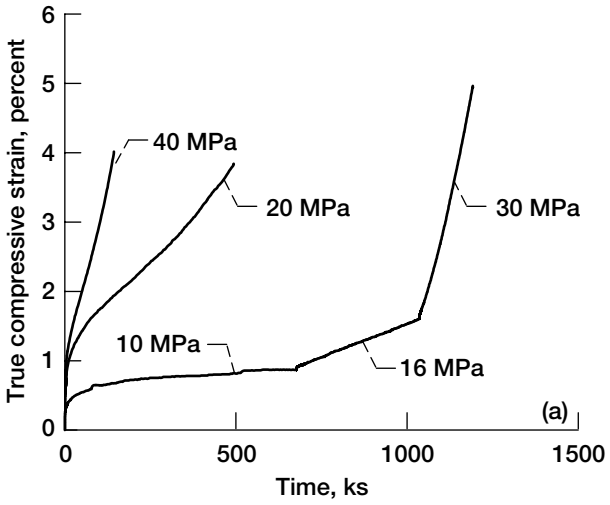

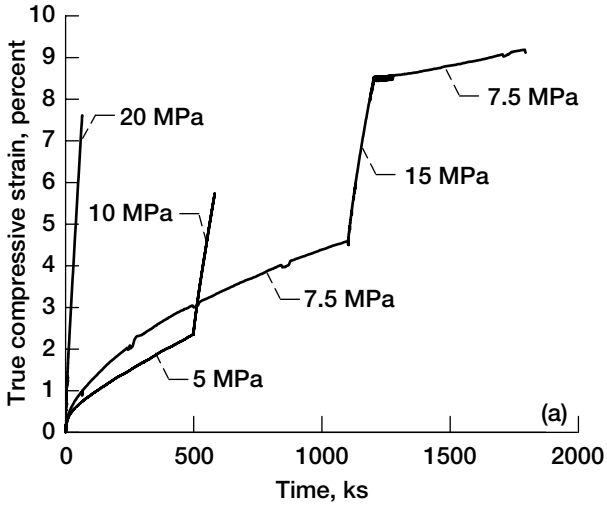

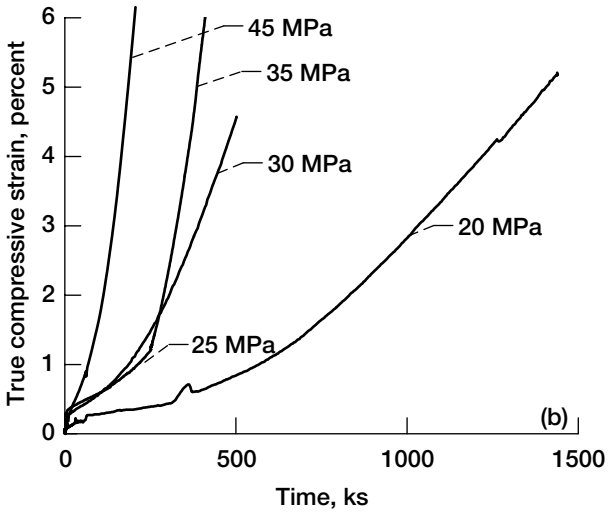

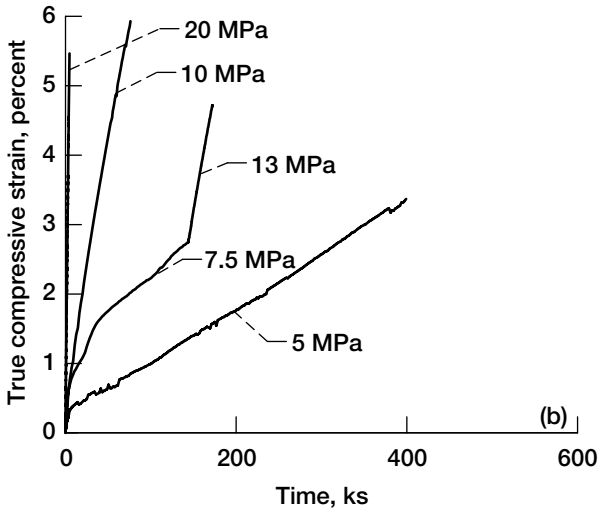

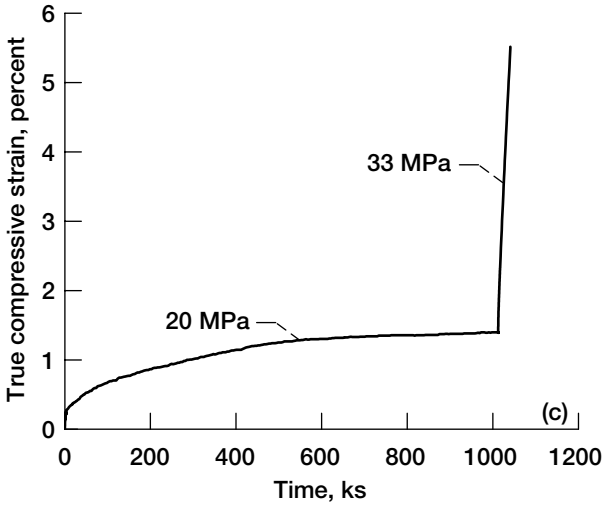

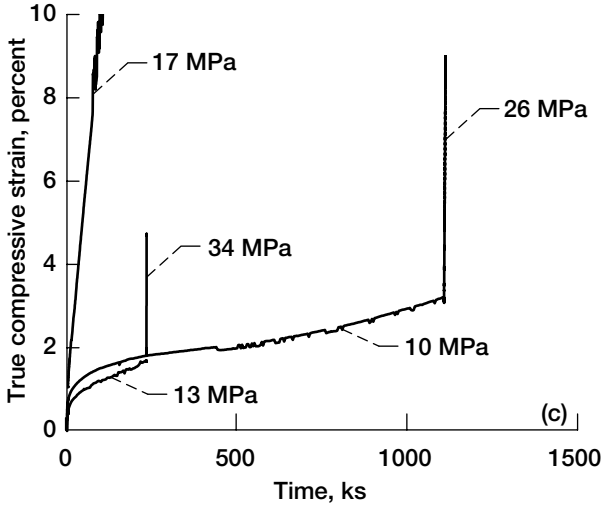

Figure 9.—Single and multiple constant load creep curves at 1400 K as a function of the engineering stress. (a) <001> NiAl-2Cr. (b) <111> NiAl-2Cr. (c) <110> NiAl-6Cr.

Figure 10.—Single and multiple constant load creep curves at 1500 K as a function of engineering stress. (a) <001> NiAl-2Cr. (b) <111> NiAl-2Cr. (c) <110> NiAl-6Cr.

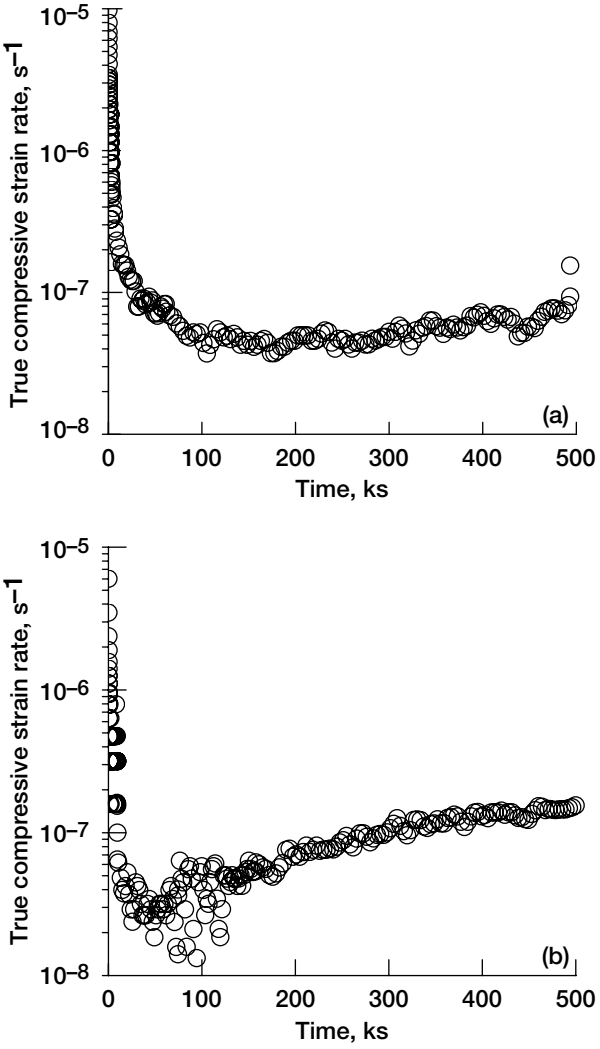

Figure 11.—Instantaneous true compressive strain rate-time curves for NiAl-2Cr creep tested at 1400 K as a function of the engineering stress. (a) <001> oriented crystal under 20 MPa. (b) <111> oriented crystal under 30 MPa.

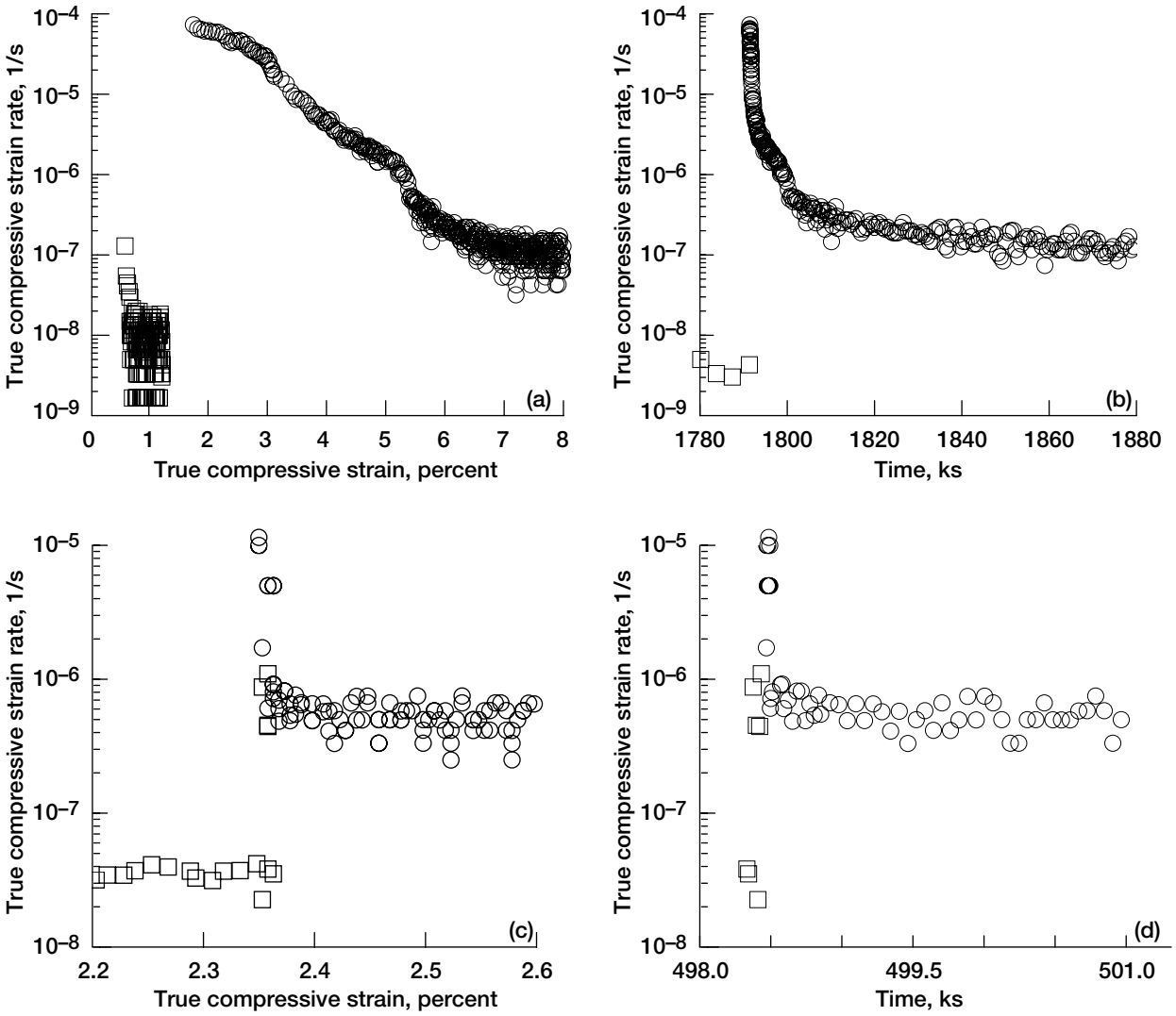

Figure 12.—Changes in the instantaneous strain rate as function of creep strain (a,c) and time (b,d) as a result of an increase in the engineering stress for <001> oriented NiAl-2Cr. (a,b) 50 to 75 MPa transition at 1300 K, and (c,d) 5 to 10.4 MPa transition at 1500 K. In all parts the open squares represent the data at the lower stress, while the open circles represent results after the load increase.

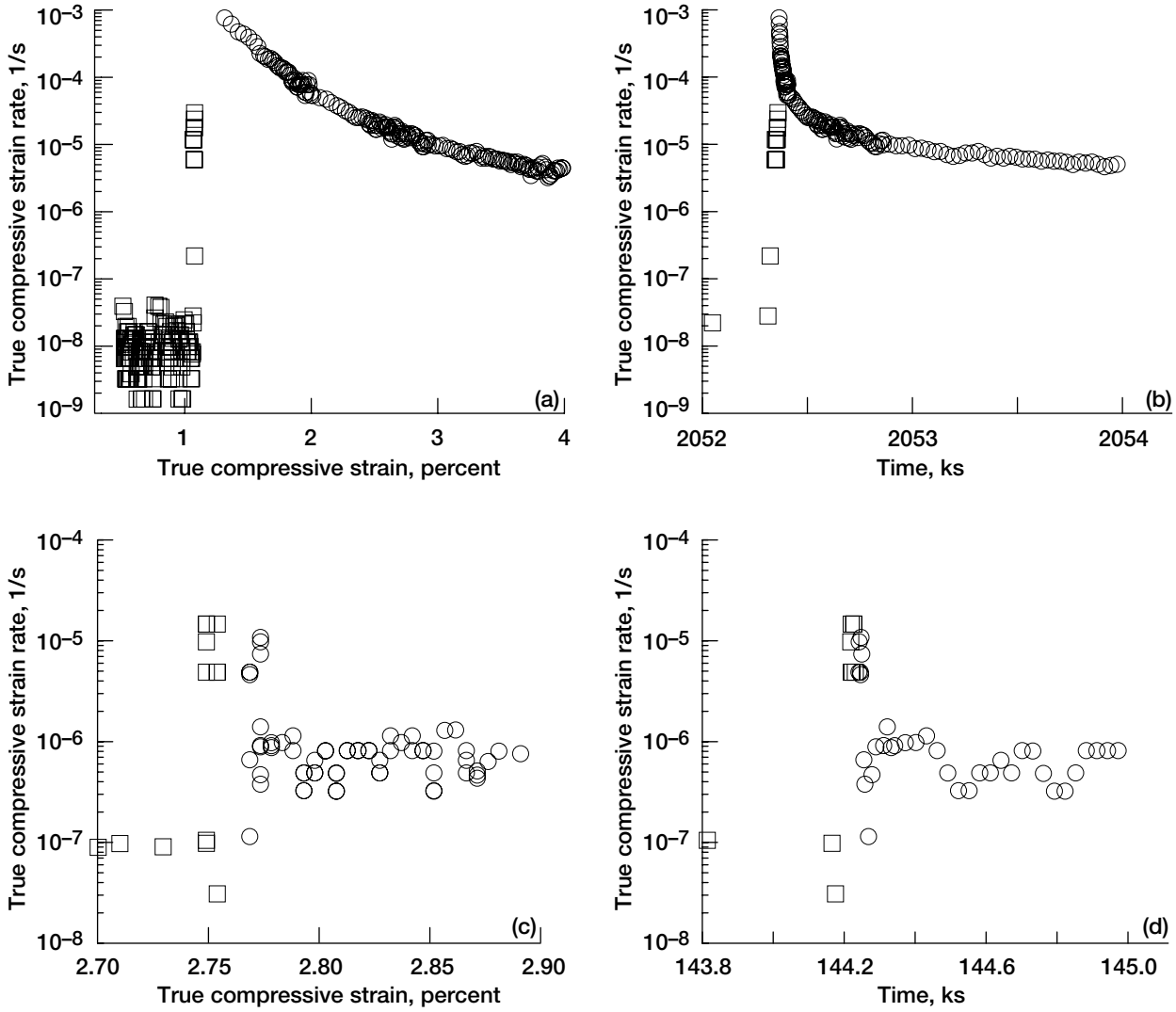

Figure 13.—Changes in the instantaneous strain rate as function of creep strain (a,c) and time (b,d) as a result of an increase in the engineering stress for <111> oriented NiAl-2Cr. (a,b) 98 to 134 MPa transition at 1200 K, and (c,d) 7.5 to 13 MPa transition at 1500 K. In all parts the open squares represent the data at the lower stress, while the open circles represent results after the load increase.

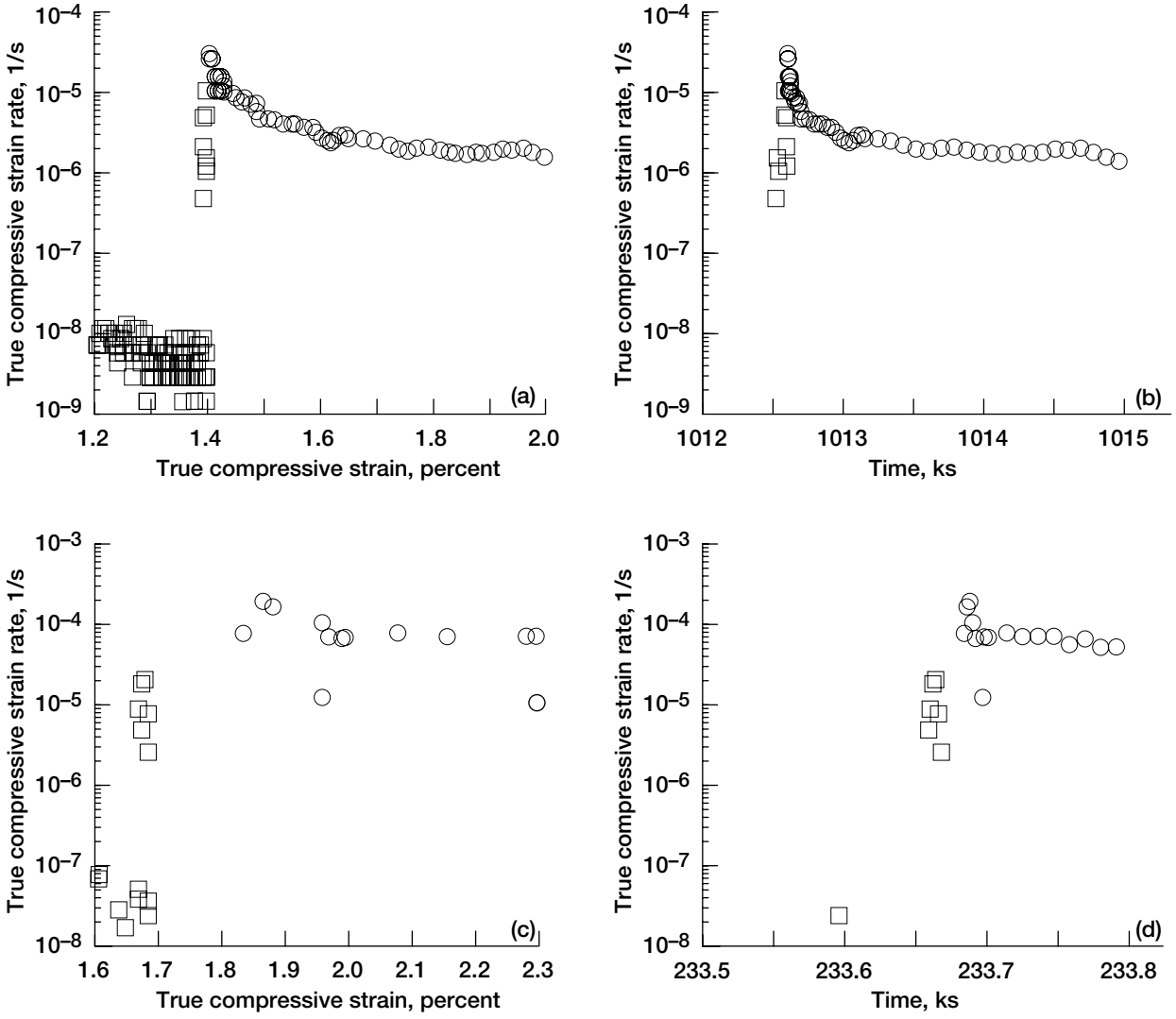

Figure 14.—Changes in the instantaneous strain rate as function of creep strain (a,c) and time (b,d) as a result of an increase in the engineering stress for <011> oriented NiAl-2Cr. (a,b) 20 to 33 MPa transition at 1400 K, and (c,d) 13 to 34 MPa transition at 1500 K. In all parts the open squares represent the data at the lower stress, while the open circles represent results after the load increase.

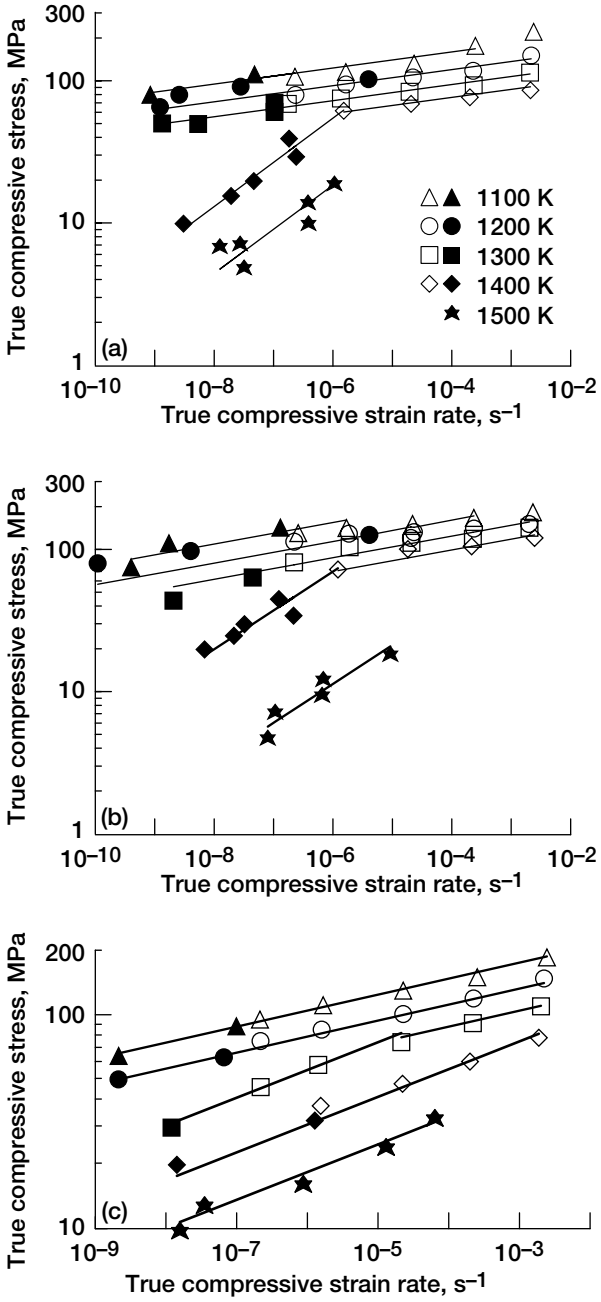

Figure 15.—True compressive flow stress-strain rate-temperature behavior. (a) <001> oriented NiAl-2Cr. (b) <111> oriented NiAl-2Cr. (c) <011> oriented NiAl-6Cr.

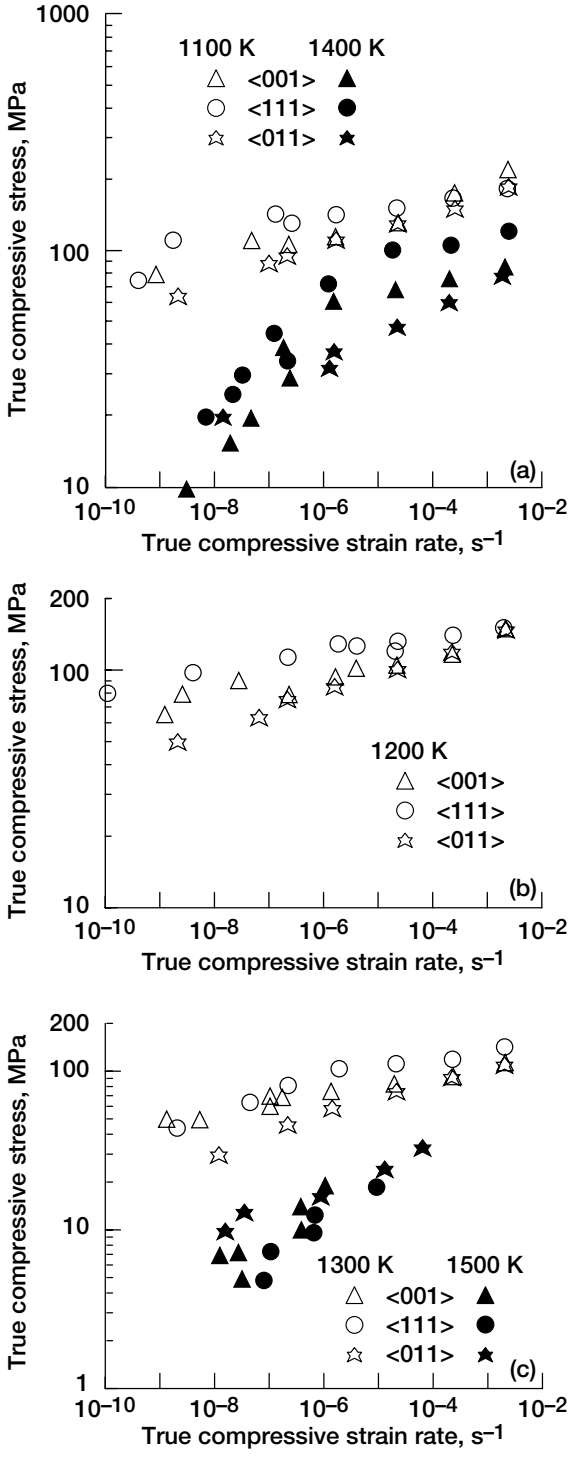

Figure 16.—Comparison of the true compressive flow stress-strain rate-temperature behavior for <001> oriented NiAl-2Cr, <111> oriented NiAl-2Cr, and <011> oriented NiAl-6Cr. (a) 1100 and 1400 K. (b) 1200 K. (c) 1300 and 1500 K.

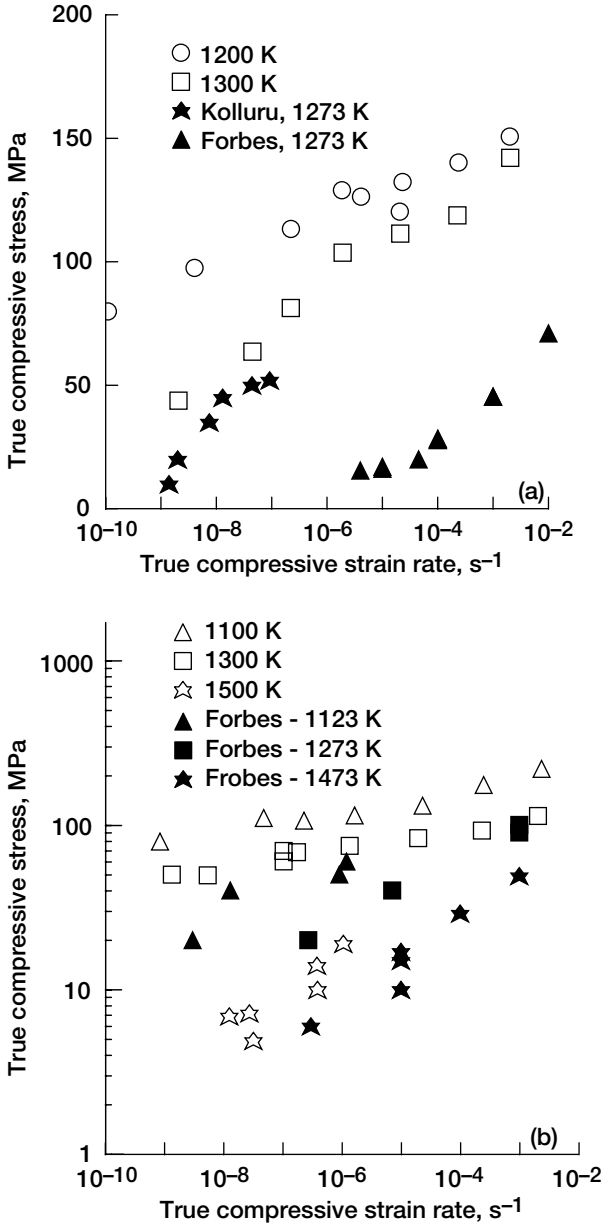

Figure 17.—Comparison of the true compressive flow stress-strain rate-temperature behavior for NiAl-2Cr and NiAl single crystals. (a) Semi-logarithm plot of data from <111>-samples tested between 1200 and 1300 K, where open symbols represent results for NiAl-2Cr from the current study; filled stars defined Kolluru's [4] values for NiAl-2Cr at 1273 K and filled triangles signify Forbes' et al. [19] NiAl behavior at 1273 K. (b) log-log representation of <001>-oriented NiAl-2Cr (open symbols) and NiAl (filled symbols, [19]) specimens at temperatures near 1100,1300, and 1500 K.

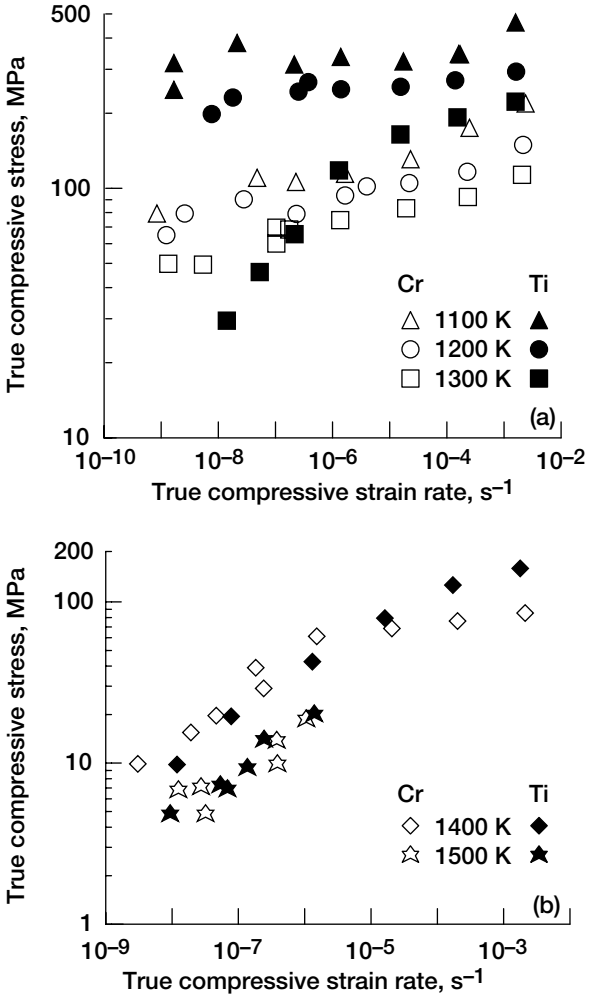

Figure 18.—Comparison of the elevated temperature compressive deformation behavior of <001>-oriented NiAl-2Cr (open symbols) and NiAl-3.6Ti [27] (filled symbols) single crystals. (a) 1100 to 1300 K. (b) 1400 and 1500 K.

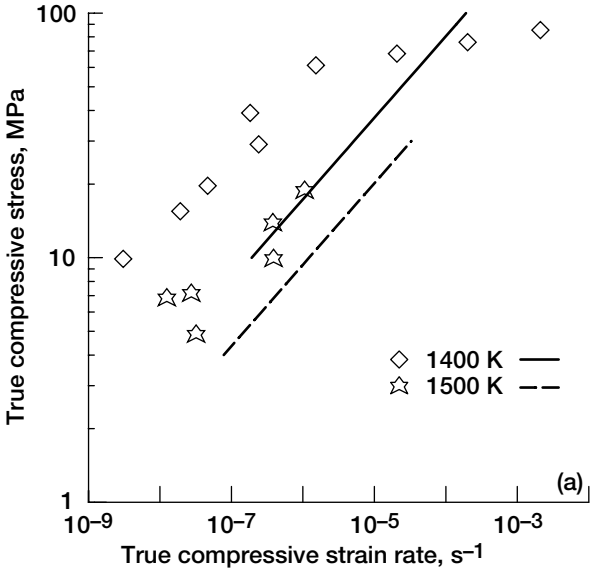

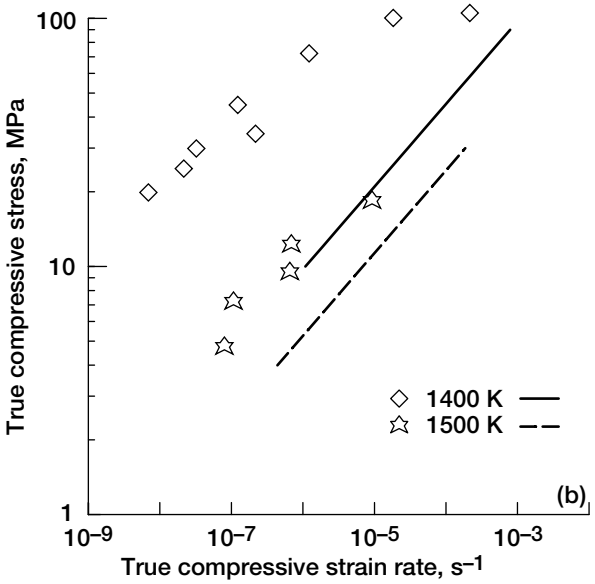

Figure 19.—Comparison of the elevated temperature compressive deformation behavior of (a) <001>- and (b) <111>-oriented NiAl-2Cr single crystals at 1400 and 1500 K (open symbols) to predicted Cottrell-Jaswon creep rates (curves).

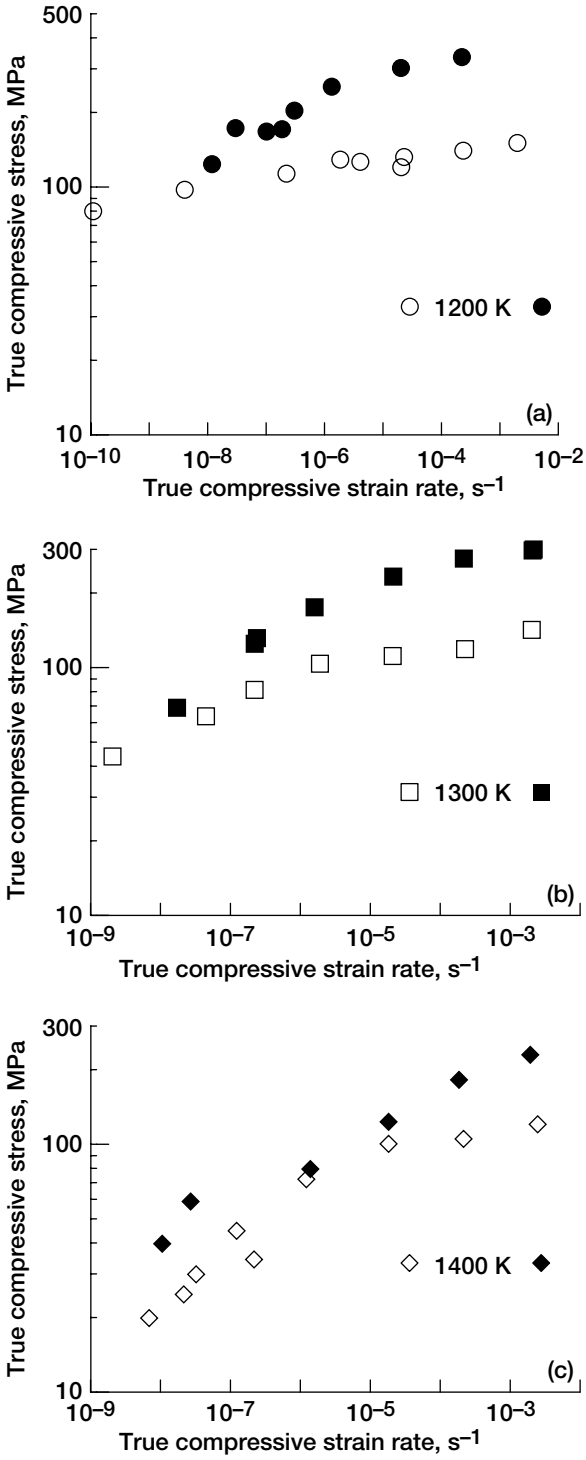

Figure 20.—Comparison of the elevated temperature compressive deformation behavior directionally solidified NiAl-33Cr-1Mo (open symbols, [12]) and <111>-oriented NiAl-2Cr single crystals (open symbols). (a) 1200 K. (b) 1300 K. (c) 1400 K.

REPORT DOCUMENTATION PAGE

Form Approved
OMB No. 0704-0188

1. AGENCY USE ONLY (*Leave blank*)	2. REPORT DATE	3. REPORT TYPE AND DATES COVERED
	September 2003	Technical Memorandum

4. TITLE AND SUBTITLE

1100 to 1500 K Slow Plastic Compressive Behavior of NiAl-xCr Single Crystals

5. FUNDING NUMBERS

WBS–22–708–31–04

6. AUTHOR(S)

J. Daniel Whittenberger and Ram Darolia

7. PERFORMING ORGANIZATION NAME(S) AND ADDRESS(ES)

National Aeronautics and Space Administration
John H. Glenn Research Center at Lewis Field
Cleveland, Ohio 44135–3191

8. PERFORMING ORGANIZATION REPORT NUMBER

E–14033

9. SPONSORING/MONITORING AGENCY NAME(S) AND ADDRESS(ES)

National Aeronautics and Space Administration
Washington, DC 20546–0001

10. SPONSORING/MONITORING AGENCY REPORT NUMBER

NASA TM—2003-212488

11. SUPPLEMENTARY NOTES

J. Daniel Whittenberger, NASA Glenn Research Center; and Ram Darolia, GE Aircraft Engines, Cincinnati, Ohio 45215. Responsible person, J. Daniel Whittenberger, organization code 5120, 216–433–3196.

12a. DISTRIBUTION/AVAILABILITY STATEMENT

Unclassified - Unlimited
Subject Category: 26 Distribution: Nonstandard

Available electronically at http://gltrs.grc.nasa.gov

This publication is available from the NASA Center for AeroSpace Information, 301–621–0390.

12b. DISTRIBUTION CODE

13. ABSTRACT ***(Maximum 200 words)***

The compressive properties of near <001> and <111> oriented NiAl-2Cr single crystals and near <011> oriented NiAl-6Cr samples have been measured between 1100 and 1500 K. The 2Cr addition produced significant solid solution strengthening in NiAl, and the <111> and <001> single crystals possessed similar strengths. The 6Cr crystals were not stronger than the 2Cr versions. At 1100 and 1200 K plastic flow in all three Cr-modified materials was highly dependent on stress with exponents > 10. The <011> oriented 6Cr alloy exhibited a stress exponent of about 8 at 1400 and 1500 K; whereas both <001> and <111> NiAl-2Cr crystals possessed stress exponents near 3 which is indicative of a viscous dislocation glide creep mechanism. While the Cottrell-Jaswon solute drag model predicted creep rates within a factor of 3 at 1500 K for <001>-oriented NiAl-2Cr; this mechanism greatly over predicted creep rates for other orientations and at 1400 K for <001> crystals.

14. SUBJECT TERMS

Nickel aluminide; NiAl; Single crystals; High temperature mechanical properties; Creep

15. NUMBER OF PAGES
35

16. PRICE CODE

17. SECURITY CLASSIFICATION OF REPORT	18. SECURITY CLASSIFICATION OF THIS PAGE	19. SECURITY CLASSIFICATION OF ABSTRACT	20. LIMITATION OF ABSTRACT
Unclassified	Unclassified	Unclassified	